METAMATERIAL-INSPIRED RECONFIGURABLE SERIES-FED ARRAYS

A Dissertation
Submitted to the Graduate Faculty
of the
North Dakota State University
of Agriculture and Applied Science

By

Bilal Ijaz

In Partial Fulfillment of the Requirements
for the Degree of
DOCTOR OF PHILOSOPHY

Major Department:
Electrical and Computer Engineering

April 2014

Fargo, North Dakota

North Dakota State University
Graduate School

Title

Metamaterial-inspired Reconfigurable Series-fed Arrays

By

Bilal Ijaz

The Supervisory Committee certifies that this ***disquisition*** complies with North Dakota State University's regulations and meets the accepted standards for the degree of

DOCTOR OF PHILOSOPHY

SUPERVISORY COMMITTEE:

Dr. Benjamin D. Braaten
Chair

Dr. David A. Rogers

Dr. Ivan T. Lima

Dr. Orven F. Swenson

Approved:

04/29/2014
Date

Dr. Scott C. Smith
Department Chair

ABSTRACT

One of the biggest challenges in modern day wireless communication systems is to attain agility and provide more degrees of freedom in parameters such as frequency, radiation pattern and polarization. Existing phased array antenna technology has limitations in frequency bandwidth and scan angle. So it is important to design frequency reconfigurable antenna arrays which can provide two different frequency bandwidths with a broadside radiation pattern having a lower sidelobe and reduced frequency scanning.

The reconfigurable antenna array inspired by the properties of metamaterials presented here provides a solution to attain frequency agility in a wireless communication system. The adaptive change in operating frequency is attained by using RF p-i-n diodes on the antenna array. The artificially made materials having properties of negative permeability and negative permittivity have antiparallel group and phase velocities, and, in consequence of that, they support backward wave propagation. The key idea of this work is to demonstrate that the properties of metamaterial non-radiating phase shifting transmission lines can be utilized to design a series-fed antenna array to operate at two different frequency bands with a broadside radiation pattern in both configurations. In this research, first, a design of a series-fed microstrip array with composite right/left-handed transmission lines (CRLH-TLs) is proposed. To ensure that each element in the array is driven with the same voltage phase, dual-band CRLH-TLs are adopted instead of meander-line microstrip lines

to provide a compact interconnect with a zero phase-constant at the frequency of operation. Next, the work is extended to design a reconfigurable series-fed antenna array with reconfigurable metamaterial interconnects, and the expressions for array factor are derived for both switching bands.

ACKNOWLEDGMENTS

First of all I would like to thank Almighty Allah for His uncountable blessings on me.

I would like to express my sincere thanks to Dr. Benjamin D. Braaten for providing immense guidance and supervision throughout my studies and research at North Dakota Sate University.

I am really grateful to Prof. David A. Rogers, Prof. Ivan T. Lima and Prof. Orven F. Swenson for serving on my graduate committee.

I would also like to thank all my applied electromagnetics group members for their collaboration during research. Finally, I would like to express special thanks to my family for their support and encouragement.

DEDICATION

To my family and beloved teachers.

TABLE OF CONTENTS

LIST OF TABLES

LIST OF FIGURES

LIST OF SYMBOLS

λ_o ..... free space wavelength

λ_g ..... guided wavelength

θ ..... angle from broadside

Φ_o ..... progressive phase shift

μ ..... magnetic permeability

ϵ ..... electrical permittivity

μ_o ..... free space permeability

ϵ_o ..... free space permittivity

μ_r ..... relative permeability

ϵ_r ..... relative permittivity

γ ..... complex propagation constant

α ..... attenuation constant

β ..... propagation constant

ω ..... angular frequency

Φ_{RH} ..... phase incurred by right-handed transmission line

Φ_{LH} ..... phase incurred by left-handed transmission line

Φ_{Total} ..... Total phase incurred by transmission line

β_{LH} ..... propagation constant of left-handed transmission line

CHAPTER 1. INTRODUCTION

1.1. Motivation

An antenna is an integral part in any communication or radar system, acting as a transformer between the electromagnetic wave propagating in free space and guided electromagnetic wave at the receiving or transmitting end. There are several different categories of antennas such as, dipole antennas, horn antennas, microstrip antennas, log-periodic antennas, or reflector antennas. These types of antennas possess different benefits for different types of applications. In order to improve the overall system performance and achieve multi-band capabilities, it is necessary to develop antennas which can be reconfigured by changing their fundamental operating characteristics. With the development of artificial negative refractive index metamaterials, which offers unique electromagnetic properties, it is now possible to overcome some of the design constraints in developing reconfigurable antenna arrays.

1.2. Background

Antennas are essential for any communication medium which uses electromagnetic waves as a propagation mechanism. With the advent of printed antenna technology in the 1950s [1], there has been an extensive amount of research carried out in printed antennas and arrays. Printed patch antenna arrays are currently used in satellite communications [2]−[4] and wireless systems for their attractive features such as light weight, small size, low cost, improved directivity and obtaining a desired radiation pattern which is not achievable in single element configurations [5]. The microstrip patch antennas are classified as low to moderate gain antennas, and they usually have a gain ranging from 5 to 8 dBi when used in single-element configurations. The microstrip radiator concept and its use with a linear multi-feed array was published by Munson [6]. In general the microstrip radiating element is formed using a conducting sheet above a ground plane. The separation between

ground plane and the conducting sheet is a small fraction of wavelength [6].

The invention of the Yagi-Uda antenna array in 1926 opened a new gateway in array technology research followed by the mechanically steered and phased arrays around the World War II era. With the invention of electronic phase shifters, the world observed a paradigm shift in design of antenna arrays. Series-fed and parallel-fed arrays are the two most commonly used approaches in designing low profile printed antenna arrays. These feed techniques are shown in Figure 1 [4]. In the following sections, the background of series-fed arrays, reconfigurable antennas and metamaterials is presented.

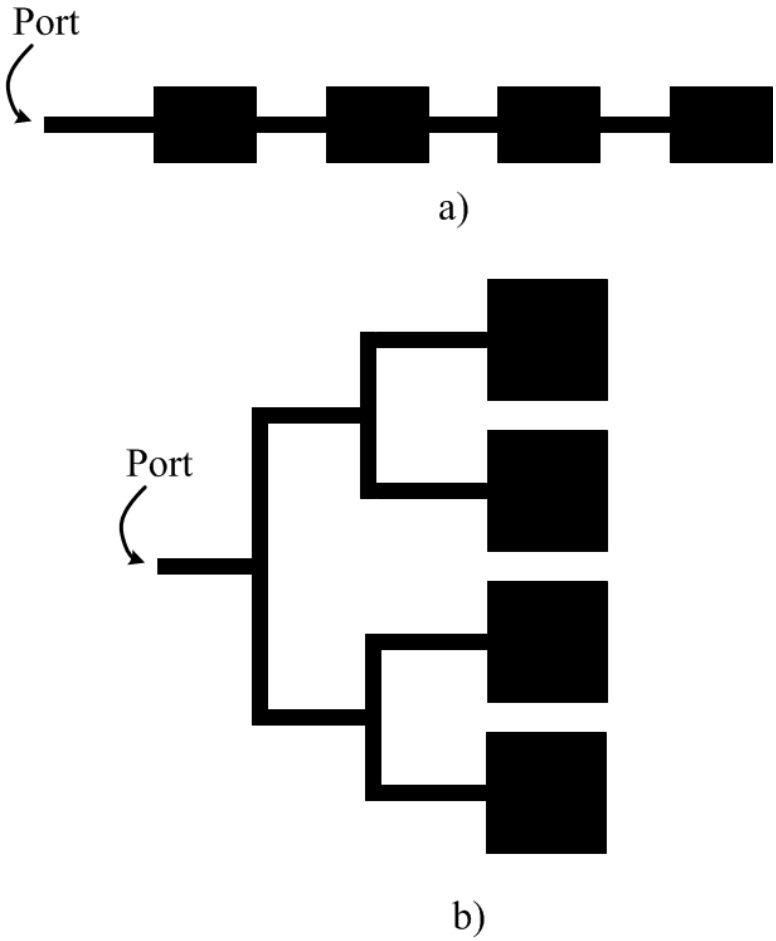

Figure 1. a) Microstrip series-fed antenna array. b) Microstrip parallel-fed antenna array.

1.2.1. Background of series-fed arrays

Antenna arrays are used to provide high directivity. In the early years microstrip half wave resonators were cascaded to form linear arrays. Several different types of microstrip arrays can be classified as the first generation of arrays developed in the 1950s, 1960s, and early 1970s era. Some of the earlier work provides four different independent solutions for lightweight and inexpensive arrays, and they included arrays such as the monolithic microstrip array developed by Munson [7], the etched broadside and endfire arrays proposed by Fubini [8]−[9], narrow line radiators proposed by James and Wilson [10] and multi-layer arrays proposed by Collings [11]−[12]. These arrays have different bandwidths and radiation characteristics, and they provided a solid foundation for further work in array technology.

There are network models by which we can calculate the dimensions for an array to obtain high gain [5], [13] and [14]. The series-fed array was the first practical realization of a microstrip patch array. The array was formed by connecting each element using the conventional right-handed transmission lines. The original series-fed array was classified as the standing-wave array. In initial years, it was designed with a waveguide, but with the passage of time microstrip lines gave much more flexibility to the design. Microstrip lines have the flexibility that the impedance can be altered by changing the size of the line and desired amplitude tapering can be achieved in the same way [15]−[16]. The phase difference between two adjacent elements in a series-fed array is given by equation [17]:

$$\phi = \frac{2\pi l}{\lambda} \tag{1.1}$$

where l is the length of the line which connects adjacent elements and λ is the operating wavelength. The direction of the main beam and the scan sensitivity is given by the following equations [18]:

$$dsin\theta + \sqrt{\epsilon}l = \lambda = c/f \tag{1.2}$$

and

$$\frac{\partial\theta}{\partial f} = -\frac{c}{df^2 cos\theta} \tag{1.3}$$

where l is the length of the line between adjacent elements, d is the spacing between the elements, c is the speed of light and θ is the beam-pointing angle which is measured from the broadside direction. The non-resonant width of the rectangular patch element is used to control the side lobe levels of the radiation pattern [18]. A typical microstrip patch antenna array is shown in Figure 2 [4].

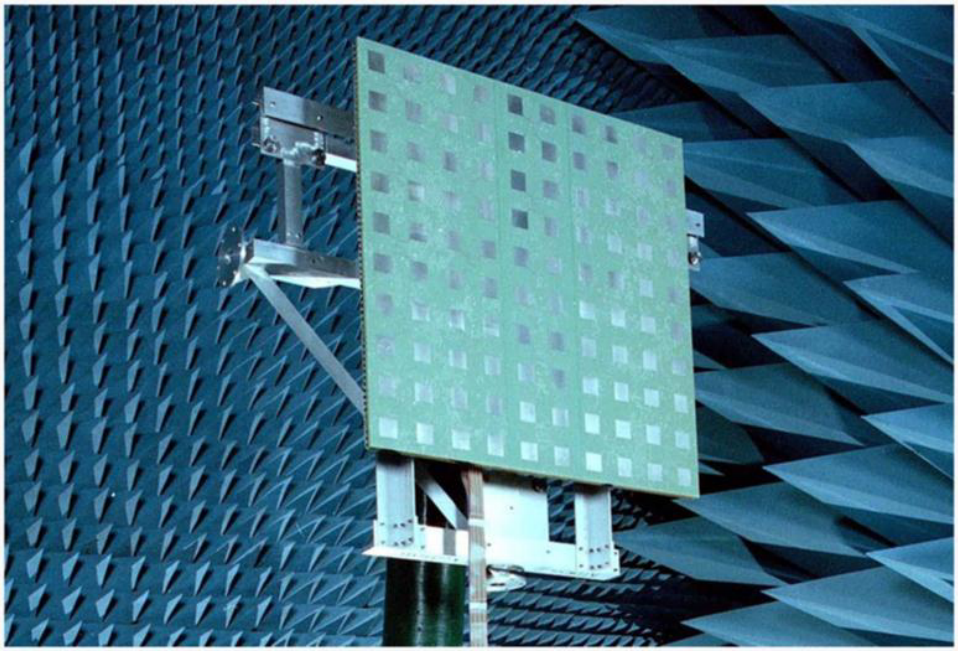

Figure 2. A microstrip patch antenna array.

The series-fed arrays implemented on a substrate have compact feed networks with lower feed-line losses [19]. The series-fed antenna arrays employing right-handed transmission line feed networks have a narrow radiation bandwidth. Due to this disadvantage, any error in the fabrication process will degrade the overall array

performance.

1.2.2. Previous work on reconfigurable antennas

Multiband capabilities are an integral part of modern day wireless communications as the spectrum has spread from a few megahertz range to frequencies above 1 GHz. Using multiple antennas to operate at different frequencies is not an efficient solution. One way to achieve the multiband capabilities is to design efficient antennas which are frequency reconfigurable, compact size, and with less complex geometry. The current literature is lacking in explaining the design guidelines for frequency reconfigurable antenna arrays, and one aspect of this research is to use the properties of metamaterials to achieve frequency reconfigurability. The first patent on reconfigurable antennas was reported in 1983 by Schaubert [22]. In 1999, a multi university program was launched by the Defense Advanced Research Projects Agency (DARPA) to investigate reconfigurable antennas and their applications [23]. According to the existing literature, there are four main categories of reconfigurable antennas [24].

1. Frequency reconfigurable antennas, where the operating or notch frequency is changed by hopping between different frequency bands. This is usually done by some tuning or notch in the antenna reflection coefficient.

2. Radiation pattern reconfigurable antennas, where the radiation pattern is tuned.

3. Polarization reconfigurable antennas, where the polarization is changed, i.e., horizontal, vertical, right hand circular polarization (RHCP), left hand circular polarization (LHCP), etc.

4. A combination of the above three categories.

Different techniques are used to achieve the frequency reconfigurable operation [25]. Some of the most common techniques are summarized below.

1. Electrically reconfigurable Antennas.

    a) Using RF-MEMS (micro-electro-mechanical systems) [26].

    b) Using PIN diodes [27].

    c) Using varactors [28].

2. Optically reconfigurable antennas.

    a) Using nonintegrated optical fibers [29].

    b) Using integrated optical fibers [30].

    c) Using integrated laser diodes [31].

3. Physically reconfigurable antennas [32].

A comparison between electrical properties of electronically and optically switching techniques is presented in Table 1 [25].

Table 1. Comparison of electrical properties.

Electrical Property	RF MEMS	PIN Diode	Optical Switch
Voltage (V)	20-100	3-5	1.8-1.9
Current (mA)	0	3-20	0-87
Power Consumption (mW)	0.05-0.1	5-100	0-50
Switching Speed	1-200 μsec	1-100 nsec	3-9 μsec
Isolation (1 to 10 GHz)	very high	high	high
Loss dB (1 to 10 GHz)	0.05-0.2	0.3-1.2	0.5-1.5

1.2.3. Previous work on metamaterials

Metamaterials exhibit certain electromagnetic properties which are not found in nature. According to Science magazine, metamaterials inspired antennas and microwave devices are among the top ten scientific breakthroughs of the last decade [34]. The metamaterials are regarded as special left-handed materials having properties of negative permeability and permittivity. The microstrip realization of metamaterials

has been developed, and it has a variety of applications in antennas and microwave devices. The transmission line approach to design metamaterials has opened gateways for further research and development in applied electromagnetics. Veselago in 1967 [37] was the first physicist who realized the concepts of left-handed materials. He investigated left-handed materials (LHM) properties like reversal of Snell's law and the Doppler Effect. LHM support electromagnetic waves with antiparallel group and phase velocities, commonly known as backward waves. The energy travels in the forward direction but the wave front travels backwards towards the source resulting in a positive phase change along the length of the transmission line [35]−[36].

Transmission line (TL) theory has been widely used as a tool to analyze a simple right handed transmission line (i.e., a microstrip of certain size on a printed circuit board). In a similar way the composite right-hand, left-hand metamaterials commonly known as CRLH have been modeled using the TL analysis techniques. In recent years, the radiated wave applications of CRLH like the zeroth order resonator antenna [38], the backfire-to-endfire leaky wave antenna [39] and electronically controlled leaky wave antenna have been reported [34]. The transmission line implementation of metamaterials is composed of shunt inductors and series capacitors arranged in a periodic manner on a printed circuit board. With the development of LC (inductance and capacitance) networks, several efforts have been made to design and analyze the CRLH metamaterials for 1-D, 2-D and 3-D metamaterials structures [34]. Some of the microwave applications of CRLH TLs include the dual-band branch line coupler, asymmetric backward-wave directional coupler and CRLH hybrid ring [34].

1.3. Current work on reconfigurable arrays

In 2001 a US patent on a reconfigurable microstrip antenna array was registered which used Micro-Electro-Mechanical System (MEMS) switches for operation at multiple frequencies [40]. In 2002, James, Chin-Chang, Yongxi and Itoh investigated a

reconfigurable leaky-wave/patch microstrip aperture for phased-array applications [41]. Long leaky-wave microstrip antennas segmented in several smaller patch antennas were used. In 2011, a circularly polarized array composed of linear polarized microstrip patches fed by a metamaterial transmission line was reported [42]. An antenna array of 2×2 was designed using four square linear polarized microstrip patches. With a survey of the existing literature, it can be seen that very little research has been carried out in frequency reconfigurable antenna arrays, and the case of metamaterials inspired frequency reconfigurable antennas has not been studied yet.

CHAPTER 2. AN INTRODUCTION TO ANTENNA ARRAYS, METAMATERIALS AND THE CONDUCTED RESEARCH

2.1. Introduction

This chapter is a brief summary of linear arrays, metamaterial transmission lines and the proposed research. The Linear Arrays section discusses the general expressions for a uniform linear array and arrays with a tapered amplitude distribution. The next two sections elaborate the right-handed and left-handed transmission lines. The proposed idea is discussed in the last section which shows that the properties of metamaterials can be employed in designing frequency reconfigurable series-fed antenna arrays.

2.2. Linear arrays

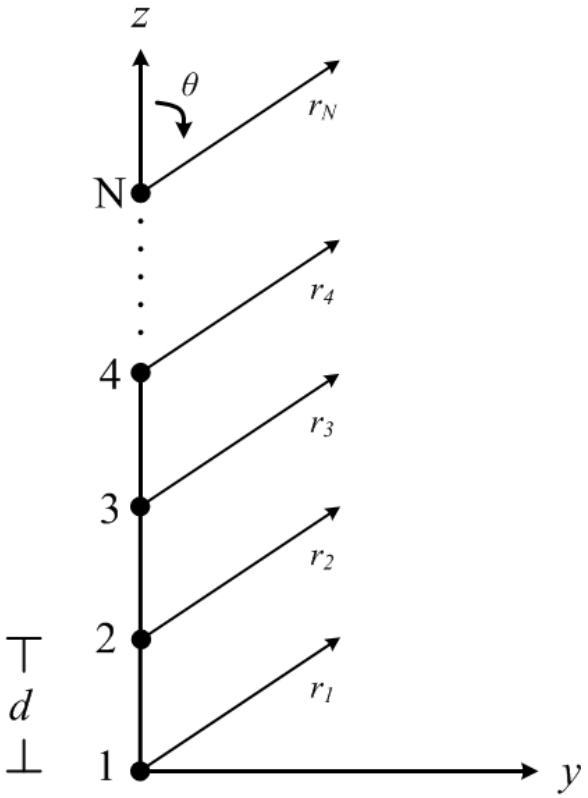

Figure 3. Far-field geometry of N-element linear array.

In order to obtain directive characteristics in a radiation pattern, the antenna

elements are arranged in a certain geometrical and electrical configuration. One such configuration is shown in Figure 3 where N antenna elements are arranged along the z-axis. Let us assume that all elements have the same amplitudes and a progressive phase shift of Φ_o. The array factor expression for this uniform linear array is given by [4]:

$$AF = \sum_{n=1}^{N} e^{j(n-1)\psi} \tag{2.1}$$

and ψ is given by,

$$\psi = k_o d\ cos\theta + \Phi_o \tag{2.2}$$

where θ is the angle from broadside, d is the inter-element spacing and Φ_o represents the progressive phase shift. The normalized closed form array factor for a N-element linear array is given by:

$$AF = \frac{1}{N} e^{j(N-1)\frac{\psi}{2}} \times (\frac{sin\frac{N\psi}{2}}{sin\frac{\psi}{2}}) \tag{2.3}$$

when the value of ψ is zero or $\pm 2n\pi$, the array will generate a broadside radiation pattern. Thus, the scan angle of a uniform linear array is given by [47]:

$$ScanAngle = sin^{-1}(-\frac{\Phi_o}{k_o d}). \tag{2.4}$$

For series-fed antenna arrays, the spacing between array elements is uniform but the excitation amplitude distribution is not uniform. In this case, the normalized array factor for an even number of array elements becomes [4]:

$$AF_{even} = \sum_{n=1}^{M} a_n\ cos(\frac{(2n-1)}{2}\ kd\ cos\ \theta). \tag{2.5}$$

And for odd numbers of array elements the normalized array factor is given by [4]:

$$AF_{odd} = \sum_{n=1}^{M+1} a_n \; cos((n-1) \; kd \; cos \; \theta) \tag{2.6}$$

where a_n is the amplitude coefficient of the antenna array.

2.3. Metamaterials

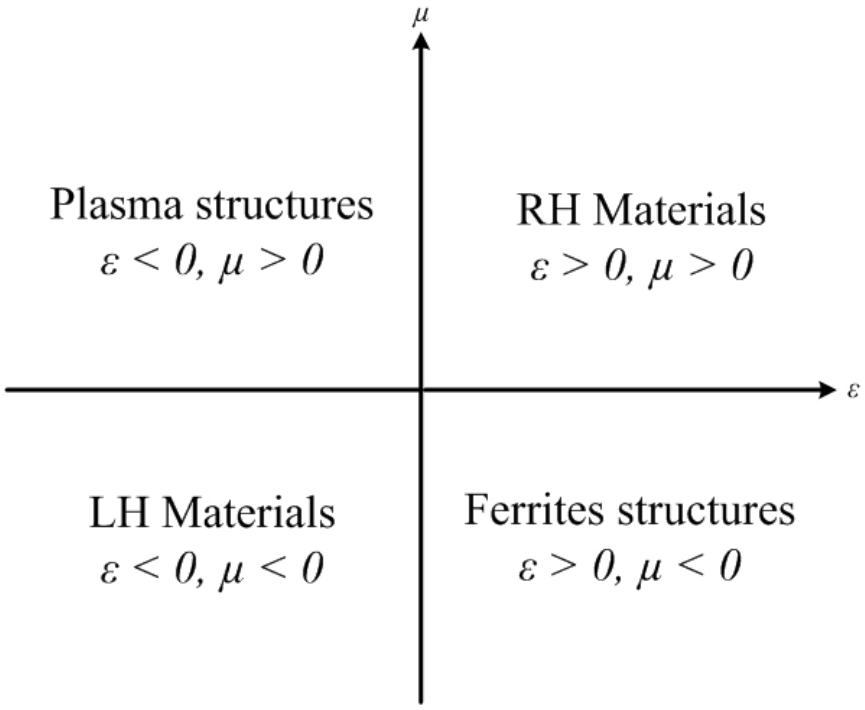

Figure 4. Permittivity-permeability diagram for right-handed materials, plasma structures, ferrite structures and left-handed materials.

In the following section, the transmission line theory of metamaterials is presented. Electromagnetic field analysis and transmission line circuit analysis techniques are used for defining the circuit models of metamaterials lines. The metamaterials are defined as "artificial effectively homogeneous electromagnetic structures with unusual properties not found in nature" [35]. Electrical permittivity ($\epsilon = \epsilon_o \epsilon_r$) and magnetic permeability ($\mu = \mu_o \mu_r$) are two important parameters by which the behavior of electromagnetic wave in a media is described [35] and [36]. The ratio of the speed of light and phase velocity in a medium is defined as the index of refraction,

and it is given by [36],

$$n = \pm\sqrt{\epsilon_r \mu_r} \tag{2.7}$$

and depending upon the positive or negative value of permittivity and permeability the above equation can have four possible scenarios which are depicted in Figure 4. The equivalent circuits for purely right-handed and left-handed transmission lines are shown in Figure 5.

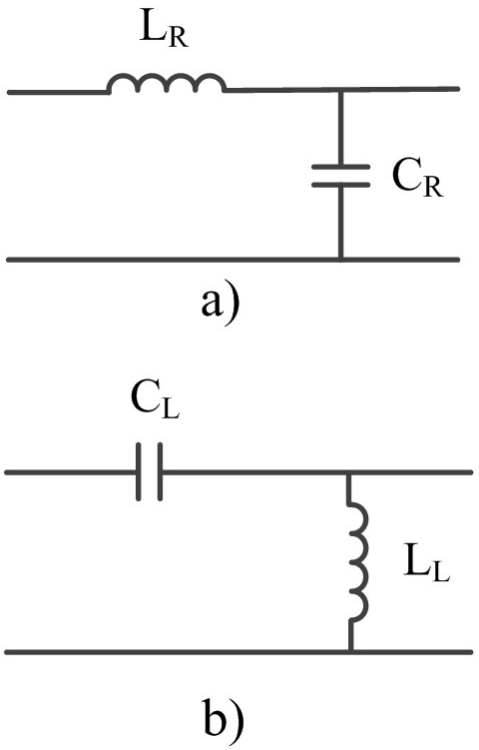

Figure 5. a) Equivalent circuit of a right-handed transmission line unit cell b) Equivalent circuit of a left-handed transmission line unit cell.

2.3.1. Right-handed transmission lines

The electric, magnetic and wave vector ($\bar{E}, \bar{H}$ and $\bar{k}$) form a right-handed triplet in right handed transmission lines. From an electromagnetic fields point of view the direction of power flow is the same as the direction of wave propagation ensuring a positive index of refraction. In microwave theory, the distributed lumped element

circuit model is used to describe the behavior of a right handed transmission line. The unit cell shown in Figure 6 has four circuit parameters namely, series resistance per unit length, series inductance per unit length, shunt conductance per unit length and shunt capacitance per unit length. For a general lossless case using the telegrapher's equation, the current and voltage on the unit cell is given by [33],

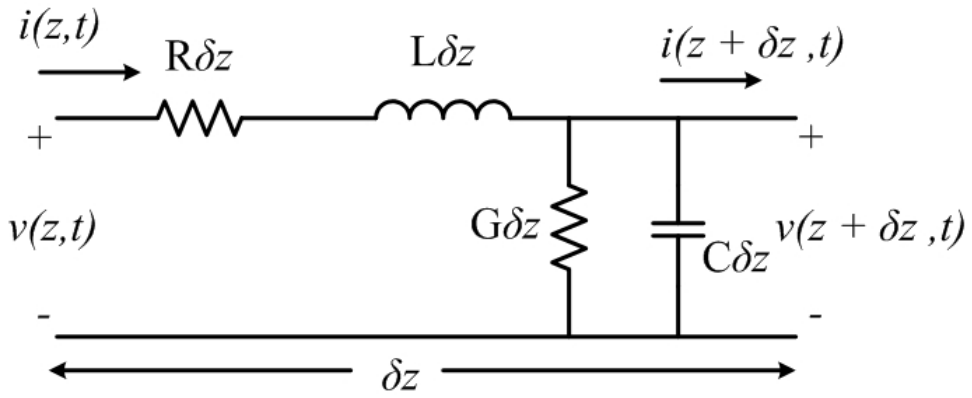

Figure 6. Equivalent circuit for an incremental length of transmission line.

$$\frac{dI(z)}{dz} = -j\omega LV(z) \tag{2.8}$$

and

$$\frac{dV(z)}{dz} = -j\omega CI(z). \tag{2.9}$$

The complex propagation constant γ is defined as,

$$\gamma = \alpha + j\beta = j\omega\sqrt{LC} \tag{2.10}$$

where the propagation constant is given as $\beta = \omega\sqrt{LC}$ and the attenuation constant $\alpha = 0$. The characteristic impedance of the lossless right-handed transmission line is given as,

$$Z_0 = \sqrt{Z/Y} = \sqrt{L/C} \tag{2.11}$$

where Z is the per unit length impedance and Y is the per unit length admittance defined as $Z = j\omega L$ and $Y = j\omega C$. The phase added by the right-handed transmission line along the length of the line d is given as [33] and [47]:

$$\Phi_{RH} = -\beta d = -\omega\sqrt{LC}d. \tag{2.12}$$

The phase velocity is given as,

$$v_p = \frac{\omega}{\beta} = \frac{1}{LC}. \tag{2.13}$$

So it can be concluded that the phase velocity as well as the group velocity for right handed transmission lines is a positive quantity, and the wave and power flows in the same positive direction which is consistent with $\bar{S} = \bar{E} \times \bar{H}$.

2.3.2. Left-handed transmission lines

The medium where the electric, magnetic and wave vector ($\bar{E}, \bar{H}$ and $\bar{k}$) form a left-handed triplet is termed as a left-handed or negative refractive index media. In such media we have anti-parallel group and phase velocities because the direction of power flow and direction of wave propagation are opposite. Such types of electromagnetic properties are not found in nature, but there are certain ways to fabricate these materials [34]. As L and C in the transmission line model are directly related to magnetic permeability and electrical permittivity, switching the roles of L and C in a transmission line model yields a virtual negative index of refraction. The new parameters are called the left-handed shunt inductance L_L and left-handed series capacitance C_L. The telegrapher equation now becomes [47],

$$\frac{dI(z)}{dz} = -(\frac{1}{j\omega L_L})V(z) \tag{2.14}$$

and

$$\frac{dV(z)}{dz} = -(\frac{1}{j\omega C_L})I(z). \tag{2.15}$$

The propagation constant for left handed or backward waves is given by [47],

$$\beta_{LH} = -(\frac{1}{\omega\sqrt{L_L C_L}}) \tag{2.16}$$

and the characteristic impedance is given by,

$$Z_{LH} = \sqrt{\frac{L_L}{C_L}} \tag{2.17}$$

and the phase incurred by the left handed transmission line is given by,

$$\Phi_{LH} = -\beta d = \frac{1}{\omega\sqrt{L_L C_L}}. \tag{2.18}$$

Lastly, the phase velocity of a left handed transmission line is a negative quantity which yields a negative index of refraction and is given as [47]:

$$v_{p,LH} = -\omega^2\sqrt{L_L C_L}. \tag{2.19}$$

Although the phase velocity in the above expression is a negative quantity, the group velocity is a positive quantity i.e., $v_{g,LH} = \omega^2\sqrt{L_L C_L}$, which shows the power still travels in a positive direction.

2.3.3. Composite right/left handed (CRLH) transmission lines

The inspection of group velocity expressions of left handed transmission lines shows that the group velocity will increase in an unbounded manner with the increase

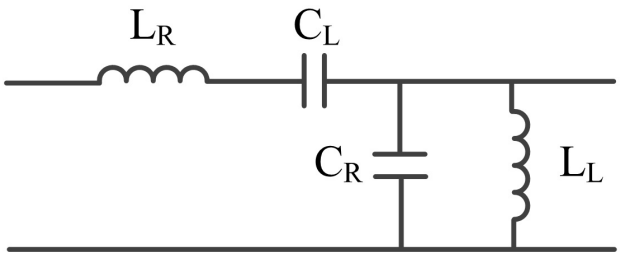

Figure 7. Equivalent circuit of a composite right/left handed transmission line unit cell.

in frequency eventually becoming more than the speed of light. It is an accepted fact that the group velocity can not exceed the speed of light ($v_g < c < v_p$). So the physical realization of purely left handed transmission line is not possible. So there is a need of adding some right-handed portion in the equivalent circuit of a left-handed transmission line which will yield the equivalent circuit shown in Figure 7. Such transmission line configurations are termed as composite right/left-hand (CRLH) transmission lines. The CRLH structure supports the forward-wave propagation above the cut-off frequency and backward-wave propagation below the cut-off frequency. The right-handed portion of the transmission line will exhibit a phase lag ($e^{-j\beta_{RH}z}$) and the left handed portion will exhibit a phase lead ($e^{+j\beta_{LH}z}$) as the wave travels along the length of transmission line. β_{RH} is a positive quantity for the right-handed medium and β_{LH} is a negative quantity for the left-handed medium. So, the total phase of this CRLH metamaterial transmission line can be expressed as [36]:

$$\Phi_{Total} = \Phi_{RH} + \Phi_{LH}. \tag{2.20}$$

From the equivalent circuit of CRLH transmission line, the per-unit length impedance and per-unit length admittance is given as,

$$Z = j(\omega L_R - \frac{1}{\omega C_L}) \tag{2.21}$$

and

$$Y = j(\omega C_R - \frac{1}{\omega L_L}). \tag{2.22}$$

Using the telegrapher equation for the above circuit, the currents and voltages are express as,

$$\frac{dI}{dz} = -j\omega(C_R - \frac{1}{\omega^2 C_L})V(z) \tag{2.23}$$

and

$$\frac{dV}{dz} = -j\omega(L_R - \frac{1}{\omega^2 L_L})I(z). \tag{2.24}$$

The characteristic impedance of the CRLH transmission line is given as,

$$Z_0 = \sqrt{\frac{L_R}{C_R}} = \sqrt{\frac{L_L}{C_L}} \tag{2.25}$$

and the series and shunt resonance frequencies are expressed as,

$$\omega_{se} = \frac{1}{\sqrt{L_R C_L}} \; and \; \omega_{sh} = \frac{1}{\sqrt{L_L C_R}}. \tag{2.26}$$

Using the phase lead and phase lag expressions of right-handed and left-handed transmission lines, we can write a general expression for phase shift per unit cell for a composite right/left-hand (CRLH) transmission line as [47]:

$$\Phi_{total} = -\omega\sqrt{L_R C_R}d + \frac{1}{\omega\sqrt{L_L C_L}}. \tag{2.27}$$

The above equation is very useful in designing the transmission lines where a certain amount of phase shift is required at a desired frequency. This is the biggest advantage of CRLH transmission lines as they can be used to provide phase lead, phase lag and even a zero phase at a desired frequency of operation. In order to understand the behavior of right handed, left handed and composite right/left handed transmission lines, a dispersion diagram is shown in Figure 8 [34] and [47]. In the next section, it is proposed that this unique property of metamaterials can be used in designing broadside reconfigurable series freed antenna arrays.

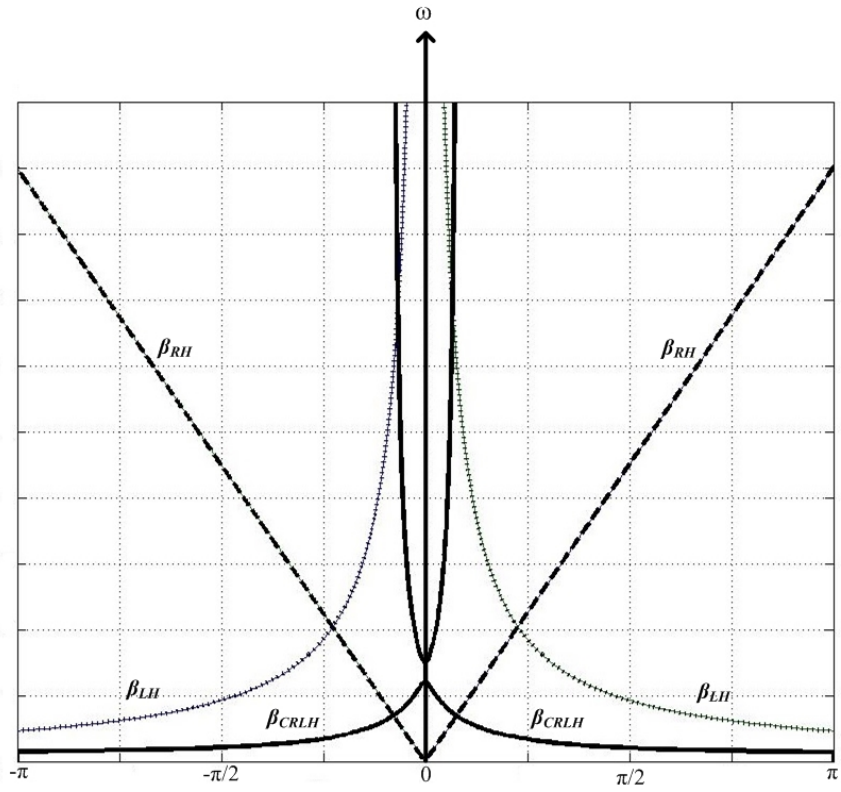

Figure 8. Dispersion diagram for purely right-handed, purely left-handed and composite right/left-handed transmission lines.

2.4. Conducted research

The metamaterials phase-shifting lines presented in [47], [49] and [36] are the motivation behind this current work as they can be used to design compact and reconfigurable antenna arrays. The feeding networks based on conventional

transmission lines are usually bulky and offer less bandwidth. In comparison, the non-radiating metamaterials phase shifting lines are fairly broadband and can be employed as the feeding networks for series-fed antenna arrays. When operated away from the designed frequency, the broadband nature of metamaterial lines helps in reducing the beam squinting effect in broadside series-fed arrays. This property of metamaterials based feed line will be helpful in obtaining the frequency reconfigurable operation of series-fed arrays. It is also worth mentioning that the phase shifting lines exhibits a phase response which is a linear function of frequency. The study of existing literature shows that these true time delay (TTD) characteristics of such lines has been implemented using various techniques [36]. But the phase shifting technique using TEM transmission line is the simplest implementation in which the insertion phase is given by [36]:

$$\phi_{TL} = -\omega\sqrt{LC}d \tag{2.28}$$

where L and C are the distributed inductance and capacitance and d is the length of transmission line. Figure 9 [49] shows a clear picture of a metamaterial transmission line implemented in a series-fed array.

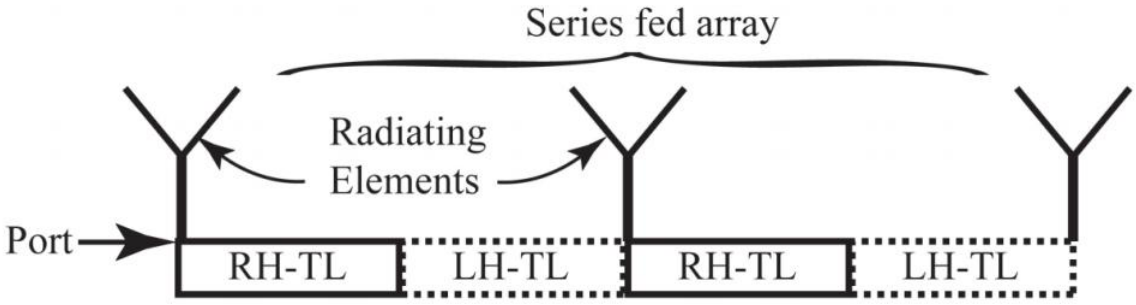

Figure 9. A series-fed array with interconnecting CRLH transmission lines.

The next section of this chapter will clearly state the research questions and design goals for research that was carried out.

2.5. Design goals and research questions

There are a variety of properties of interest in the study of series-fed antenna arrays. Some of the important properties are bandwidth, size, radiation pattern, input impedance, gain, efficiency and different feeding techniques. From the summary of chapter one it can be concluded that there is ongoing research in the area of metamaterials inspired antennas. But as this field is still emerging, there is a requirement to organize the field of reconfigurable antenna arrays and moreover there are many fundamental questions which have not been answered yet. The conducted research will answer several of those questions. As discussed in the previous section, the theory of zero phase metamaterials lines will be included in answering those questions. Due to the narrow band nature of conventional feed networks, the emerging radiation pattern in a frequency reconfigurable environment will deviate from broadside and results in an undesired phenomenon. This research focused on defining metrics for describing this phenomenon and on optimizing the frequency reconfigurable antenna array design at different frequencies of operation with a fast and efficient switching mechanism. Thus the completed research consists of simulation and measurements studies and addresses the following two questions:

- How does one design a series-fed antenna array with reconfigurable frequency operation using metamaterials?

- What are the trade-offs in the designing of such antenna arrays?

The current literature lacks in providing standard guidelines in designing of reconfigurable series-fed antenna arrays. In typical series fed-arrays, the distance between the radiating patches is kept in such a way that at the resonance frequency they provide a phase delay of 360 degrees. This phase delay of 360 degrees is essential for in-phase excitation of all radiating patches. In terms of wavelength, the length of

interconnects is kept at $\lambda/2$ of the operating frequency. The frequency and radiation characteristics of an antenna can be changed by introducing reconfigurability. The frequency response of an antenna is related to the input impedance of an antenna over frequency. An antenna can be considered to be a circuit element because of the complex input impedance i.e., $Z_{in}(\omega) = R(\omega) + jX(\omega)$. The reflection coefficient and the related parameters of the antenna such as, return loss (RL) and voltage standing-wave ratio (VSWR) depend on frequency. Usually the desired input impedance of an antenna is near 50 Ω, which gives zero reflection coefficient, unity VSWR and a return loss of infinity for a 50 Ω system. The formulas of the above three parameters are given below [51]:

$$\Gamma = \frac{Z_{in}(\omega) - Z_0}{Z_{in}(\omega) - Z_0}, \tag{2.29}$$

$$VSWR = \frac{V_{max}}{V_{min}} = \frac{1 + |\Gamma|}{1 - |\Gamma|}, \tag{2.30}$$

and

$$RL = -20\ log|\Gamma|\ (dB). \tag{2.31}$$

The total field of an array is a combination of the field emerging from a single element and a factor which is known as the array factor. The array factor for an N-element linear array is given by [4],

$$AF = \sum_{n=1}^{N} e^{j(n-1)\psi}. \tag{2.32}$$

Typically the array factor depends upon the excitation phase and geometry of the array. By varying the separation d or the phase β between the elements, we can control the array factor as well as the total field of the array. One of the important metrics in the purposed reconfigurable series-fed array design will be the

array factor. As the array is designed to operate at a certain frequency, it will be important to investigate how the array factor varies as reconfigurability is introduced in the array. When the array operates at a new frequency, the physical separation between the array elements will now change as it operates at a new wavelength. The other important metric investigated is the more directed radiation pattern, as it is the biggest advantage of the array configuration. As the antenna is operated on a new frequency, this research investigated how much variation in directivity and radiation pattern is observed as compared to the original frequency of operation. The theory of metamaterials was used to investigate their possible use in series-fed arrays design. The developed analytical expressions were used to design the antenna array. Also the procedure for determining the array factor was developed and verified by simulations and measurements. The design was tested using the commercially available software program Momentum in the Advanced Design System (ADS) [54].

CHAPTER 3. ARRAY FACTOR DERIVATION FOR RECONFIGURABLE ANTENNA ARRAY

3.1. Introduction

In this chapter, the radiation pattern expressions for a reconfigurable series-fed antenna arrays are derived. Figure 10 shows four reconfigurable dipoles which are arranged along the z-axis in a manner that the spacing d between them is a quarter of the free space wavelength at the upper switching frequency, and this physical spacing remains the same at the lower switching frequency.

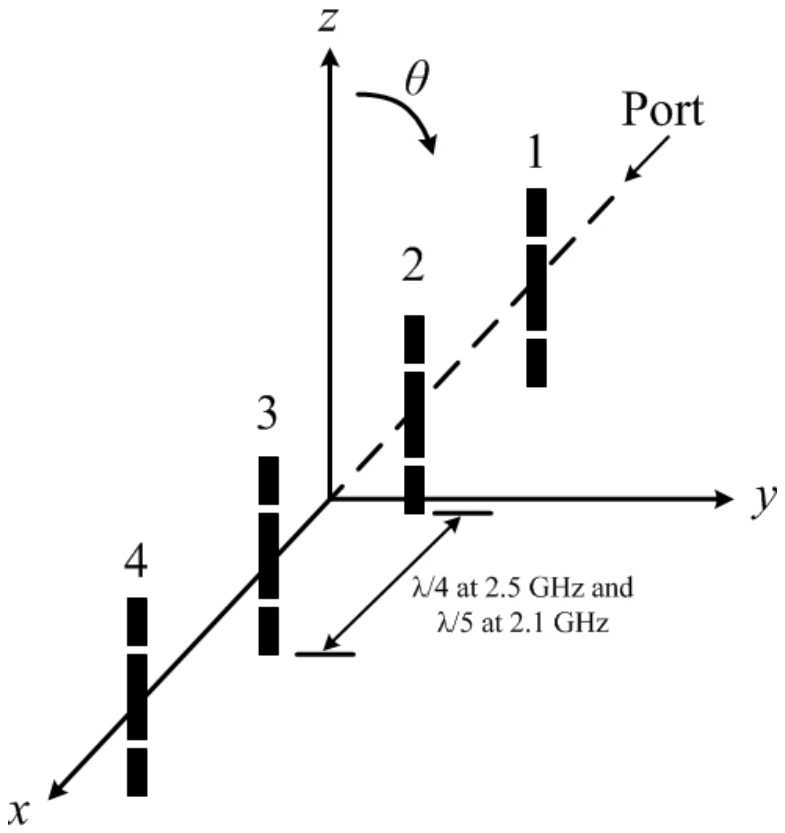

Figure 10. Four element reconfigurable metamaterial dipole array geometry.

The total field of an antenna array is equal to the single antenna element pattern times the total array factor. For a z-directed dipole, the field is not varied in its H-plane, and the variation in E-field is solely produced by the array factor of the antenna

array [47]. The new expressions for array factor at both switching frequencies are derived in the next section.

3.2. Array Factor for four-element reconfigurable antenna array

Consider the reconfigurable antenna array geometry shown in Figure 3 and Figure 10. The array factor expressions in the x-z plane are derived for both switching bands in the following manner. For the lower band configuration, the position vectors for the dipoles shown in Figure 3 are expressed as,

$$\bar{r_1} = -\frac{3}{10}\lambda_{o1}\hat{x}, \tag{3.1}$$

$$\bar{r_2} = -\frac{1}{10}\lambda_{o1}\hat{x}, \tag{3.2}$$

$$\bar{r_3} = \frac{1}{10}\lambda_{o1}\hat{x}, \tag{3.3}$$

and

$$\bar{r_4} = \frac{3}{10}\lambda_{o1}\hat{x}. \tag{3.4}$$

The unit vector for rectangular co-ordinate system is given as,

$$\hat{r} = cos\phi sin\theta\hat{x} + sin\phi sin\theta\hat{y} + cos\theta\hat{z}. \tag{3.5}$$

The general normalized array factor for dipole array is given by [4] and [47]:

$$AF = \frac{1}{N}\sum_{n=1}^{N} I_n e^{jk\hat{r}.\vec{r_n}} \tag{3.6}$$

where N is the number of antenna elements in an array, I_n is the current excitation of each element, $\hat{r}$ is the unit vector and $\bar{r_n}$ is the position vector from origin. The general form of current excitation I_n is expressed as [4] and [47]:

$$I_n = a_n e^{j(n-1)\phi_o}. \tag{3.7}$$

Now, when the array is operated at lower frequency, the physical spacing between array elements is not altered. The inter-element spacing at lower frequency becomes $\lambda_o/5$, and the new array factor equation becomes,

$$\begin{aligned} AF_{\lambda_o/5} = \frac{1}{4}(a_0 e^{-jk\frac{3}{10}\lambda_{o_1} cos\phi} + a_1 e^{j\phi_{o1}{}_{CRLH}}\, e^{-jk\frac{1}{10}\lambda_{o_1} cos\phi} + \\ a_2 e^{2j\phi_{o1}{}_{CRLH}}\, e^{+jk\frac{1}{10}\lambda_{o_1} cos\phi} + a_3 e^{3j\phi_{o1}{}_{CRLH}}\, e^{+jk\frac{3}{10}\lambda_{o_1} cos\phi}). \end{aligned} \tag{3.8}$$

In compact form, the array factor expression for the lower-band configuration can be written as,

$$AF_{\lambda_o/5} = \frac{1}{N}\sum_{q=0}^{N-1} a_n e^{jq\phi_{CRLH}}\, e^{-jk(2q+1-N)\lambda_{o_2}\cos\phi/10}. \tag{3.9}$$

where $N = 4$ is the number of elements in the array, a_n is the amplitude of the voltage driving the n^{th} element, and ϕ_{CRLH} is the phase response of the interconnecting zero-phase TL.

Now for the higher band configuration the position vectors are given as,

$$\bar{r_1} = -\frac{3}{8}\lambda_{o2}\hat{x}, \tag{3.10}$$

$$\bar{r_2} = -\frac{1}{8}\lambda_{o2}\hat{x}, \tag{3.11}$$

$$\bar{r_3} = \frac{1}{8}\lambda_{o2}\hat{x}, \tag{3.12}$$

and

$$\bar{r_4} = \frac{3}{8}\lambda_{o2}\hat{x}. \tag{3.13}$$

Using these unit vectors in the general equation of array factor gives the array factor for the upper frequency operation in the x-z plane,

$$\begin{aligned} AF_{\lambda_o/4} = \frac{1}{4}(a_0 e^{-jk\frac{3}{8}\lambda_{o_2} cos\phi} + a_1 e^{j\phi_{o2}{}_{MTM}} e^{-jk\frac{1}{8}\lambda_{o_2} cos\phi} + \\ a_2 e^{2j\phi_{o2}{}_{MTM}} e^{+jk\frac{1}{8}\lambda_{o_2} cos\phi} + a_3 e^{3j\phi_{o2}{}_{MTM}} e^{+jk\frac{3}{8}\lambda_{o_2} cos\phi}). \end{aligned} \tag{3.14}$$

The above expression can be written in compact form as,

$$AF_{\lambda_o/4} = \frac{1}{N}\sum_{q=0}^{N-1} a_n e^{jq\phi_{CRLH}} e^{-jk(2q+1-N)\lambda_{o_2}\cos\phi/8} \tag{3.15}$$

where $N = 4$ is the number of elements in the array, a_n is the amplitude of the voltage driving the n^{th} element, and ϕ_{CRLH} is the phase response of the interconnecting zero-phase TL and can be written as [47]:

$$\phi_{o_{1,2}\ CRLH} = m\left(\frac{\Delta\phi_L}{\Delta\omega}\omega + \frac{1}{\omega\sqrt{L_o C_o}}\right) + \frac{\Delta\phi_R}{\Delta\omega}\omega. \tag{3.16}$$

In (3.16), ω is the radian frequency, $\Delta\phi_R$ is the negative insertion phase due to the conventional right handed transmission line segment per $\Delta\omega$, $\Delta\phi_L$ is the phase incurred due to the CRLH portion of the transmission line per $\Delta\omega$, m represents the number of unit cells, and C_o and L_o represent the loading element values for series

capacitance and shunt inductance, respectively. The values for C_o and L_o can be computed using expressions found in [47] and [48]:

$$L_o(f_{1,2}) = Z_o \times (\frac{1}{2 \times \omega_o \times \phi_L}) \tag{3.17}$$

and

$$C_o(f_{1,2}) = \frac{1}{Z_o} \times (\frac{1}{2 \times \omega_o \times \phi_L}). \tag{3.18}$$

The expressions in (3.9) and (3.15) can now be used by a designer to (1) compute the radiation pattern of the reconfigurable array in Figure 10 and (2) determine the inter-element phase shift required to achieve a broadside radiation at the desired switching frequencies to ensure that the array does not scan with frequency. The directivity expression for non-uniformly excited equally spaced array is given as [3]:

$$D = \frac{(\sum_{k=0}^{N} A_k)^2}{\sum_{m=0}^{N} \sum_{p=0}^{N} A_m A_p \frac{sin[(m-p)\beta d]}{(m-p)\beta d}} \tag{3.19}$$

For the two switching bands, the expression can be expressed as,

$$D_{lower\ band} = \frac{(\sum_{k=0}^{N} A_k)^2}{\sum_{m=0}^{N} \sum_{p=0}^{N} A_m A_p \frac{sin[(m-p)2\pi/5]}{(m-p)2\pi/5}} \tag{3.20}$$

and

$$D_{upper\ band} = \frac{(\sum_{k=0}^{N} A_k)^2}{\sum_{m=0}^{N} \sum_{p=0}^{N} A_m A_p \frac{sin[(m-p)\pi/2]}{(m-p)\pi/2}} \tag{3.21}$$

CHAPTER 4. A SERIES-FED MICROSTRIP PATCH ARRAY WITH INTERCONNECTING CRLH TRANSMISSION LINES

4.1. Introduction

Microstrip patch antenna arrays are currently used in satellite communications and wireless systems for their attractive features such as light weight, small size, low cost, improved directivity and obtaining a desired pattern which is not achievable in single-element configurations [53]. In particular, series-fed antenna arrays have the advantage of simple geometries, compact feed networks and low feed line losses [4],[3] and [20]. Typically a series-fed array consists of a single feed point and the radiating elements are connected in series with a feed network which consists of transmission lines that are a particular factor of wavelength of the operating signal. In some instances, this factor can be achieved using meander-lines to excite all of the elements in the array with the same voltage phase to achieve broadside radiation. However, the size of the overall meander-line feed network becomes larger and more complicated as the frequency is reduced. One way to overcome this size problem is to incorporate composite right-/left-handed (CRLH) transmission lines (TLs) in the feed network of the series-fed array [34], [48] and [52].

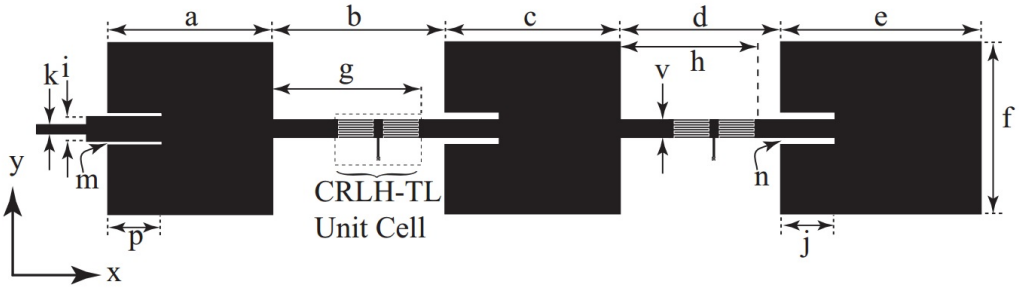

Figure 11. Layout of the cascaded CRLH RH series-fed array.

The objective of this section is to investigate the design procedure of embedding the CRLH-TLs reported in [21] into series-fed microstrip arrays. An image of the proposed series-fed array with the CRLH-TLs interconnecting each element is shown

in Figure 11. The role of the CRLH-TL in the array will be introduced in the next section. This will then be followed by simulations and measurement validations.

4.2. Zero-phase series-fed array

A series-fed antenna array is classified as a standing-wave array. The equivalent circuit of a series-fed array is shown in Figure 12(a) [20]. Here, the array is fed from the left, and Z_1, Z_2 and Z_3 represent the input impedance of the radiating elements along the length of the array. To achieve a good match at the input port, the impedance of each antenna element and interconnecting transmission lines must be chosen appropriately [3]. Furthermore, to achieve broadside radiation, each element must be fed with the same voltage phase. This can be done either by designing the length of each interconnect to be a factor of the source wavelength or to introduce CRLH-TLs that have a zero phase-constant at or near the operating frequency of interest [21]. Because of the compact size, the CRLH-TL unit-cell shown in Figure 13(a) will be used in the interconnects between the elements in Figure 12(b).

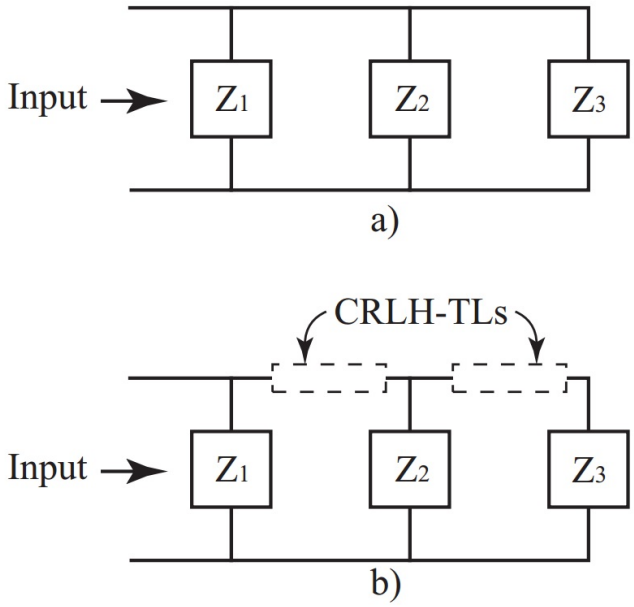

Figure 12. a) Circuit representation of a 3-element series-fed array with conventional microstrip interconnects and b) circuit representation of a 3-element series-fed array with interconnecting CRLH-TLs.

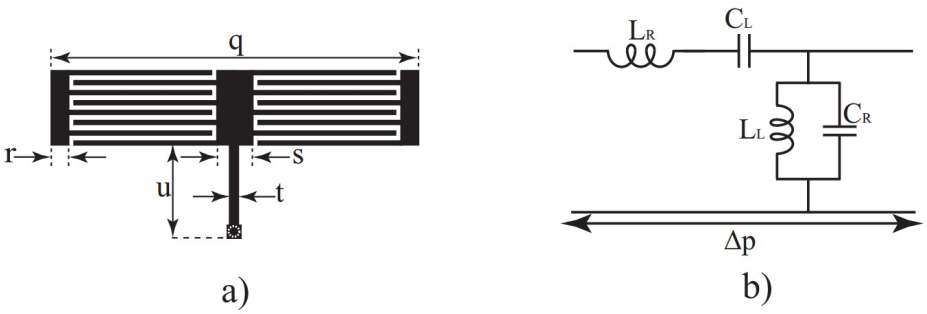

Figure 13. a) Layout of the CRLH-TL unit-cell and b) the equivalent circuit of the CRLH-TL unit-cell (q = 11.56 mm, r = 0.1 mm, s = 1.0 mm, t = 1.0 mm, u = 7.26 mm, finger length = 5.0 mm and finger gap = 0.18 mm).

The equivalent circuit of the CRLH-TL is also shown in Figure 13(b). It consists of a series reactance (consisting of L_R and C_L) as well as a shunt reactance (consisting of L_L and C_R). C_R and L_R denote the right-handed capacitance and inductance, respectively. C_R represents the parasitic capacitance between the printed conductors on the top plane and the ground (reference) plane and L_R represents the parasitic inductance of the transmission line supporting wave propagation. L_L is introduced along the length of the transmission line with shunt stubs and C_L is implemented using inter-digital capacitors (as shown in the layout in Figure 13(a)). The benefits of introducing L_L and C_L are many [7]. The property of interest to this work is when the reactance of L_L and C_L are dominant for the frequencies of interest. A positive phase shift will be introduced by the CRLH-TL unit-cell of length q. This positive phase shift can then be used in the appropriate manner to develop an interconnect with a lower zero-phase frequency. Thus, by choosing the geometry of the CRLH-TL appropriately, each element of the array can be fed with the same voltage phase for broadside radiation, and the use of meander-lines is not required.

To determine the layout of the array and achieve the required antenna impedances and interconnecting CRLH transmission line lengths, the simulation tool Momentum in the Advanced Design System (ADS) software [14] was used. The

antenna was simulated on a Rogers RT/Duroid 5880 substrate with a thickness of h = 1.57mm (ϵ_r = 2.2, $tan\ \delta$ = 0.0009). The conventional microstrip transmission line is used with the CRLH-TL as an interconnect between the patch elements in a manner similar to the dual-band lines reported in [13]. The layout of the interconnect on the 5880 substrate is shown in Figure 14.

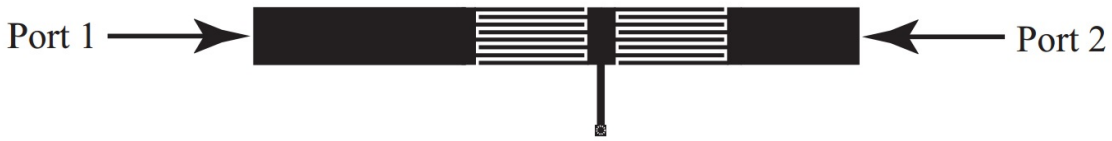

Figure 14. Layout of the CRLH-TL interconnect between the elements in the series-fed array with a length of 40.59 mm.

The dimensions of the CRLH unit-cell are shown in the caption of Figure 13, and the S_{21} phase of the total interconnect is shown in Figure 15. The first zero-phase frequency crossing occurs at f = 2.2 GHz, which is near our operating frequency of interest. For comparison, a microstrip TL with the same width at the CRLH-unit cell and length as the interconnect in Figure 14 was simulated for the same frequencies. The phase introduced by this microstrip interconnect is shown in Figure 16. The first zero-phase frequency occurs at 5.39 GHz. The zero-phase frequency of the CRLH interconnect is approximately 60 percent lower than the microstrip interconnect. This illustrates the usefulness of the compact CRLH interconnects.

Next, the interconnect (shown in Figure 14) was added to the series fed array shown in Figure 11. The design was again simulated using Rogers 5880 substrate and manufactured for testing. The manufactured prototype array is shown in Figure 17(a) with the dimensions outlined in the caption.

4.3. Simulation and measurement results

The proposed antenna array was manufactured on a 62-mil (1.57 mm) thick Rogers RT/duroid 5880 [55] grounded (double sided copper) substrate which has

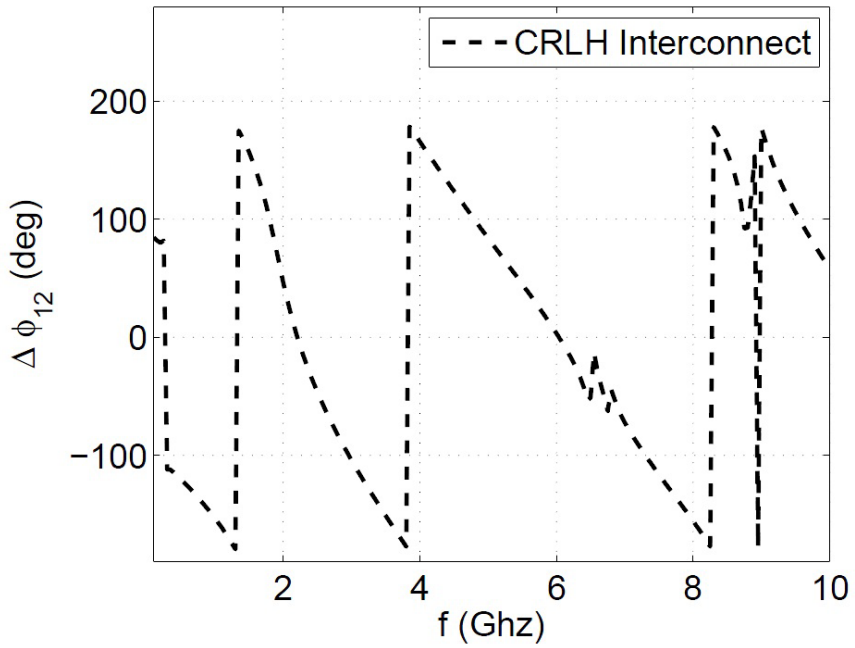

Figure 15. Simulated S_{12} phase of the CRLH interconnect.

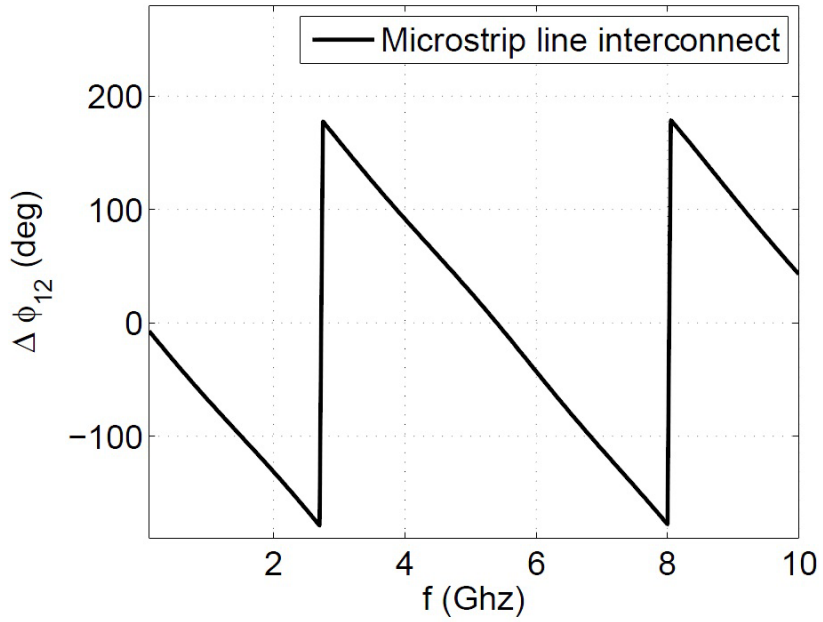

Figure 16. Simulated S_{12} phase of the conventional microstrip transmission line interconnect.

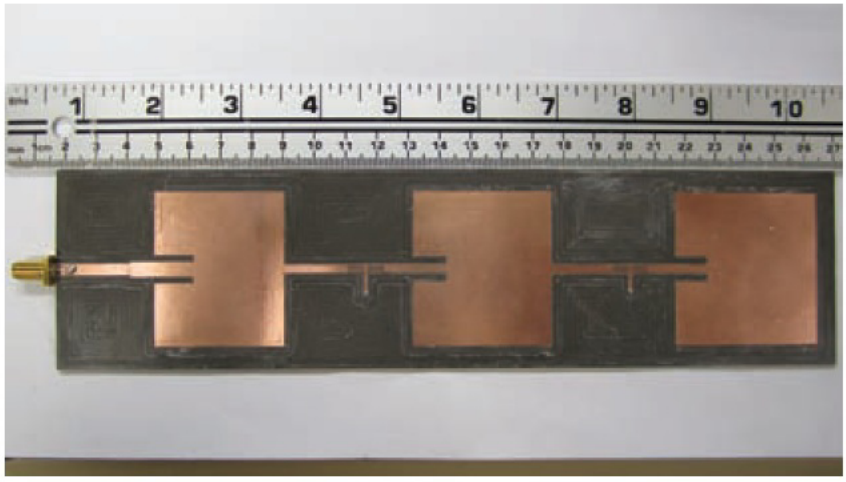

a)

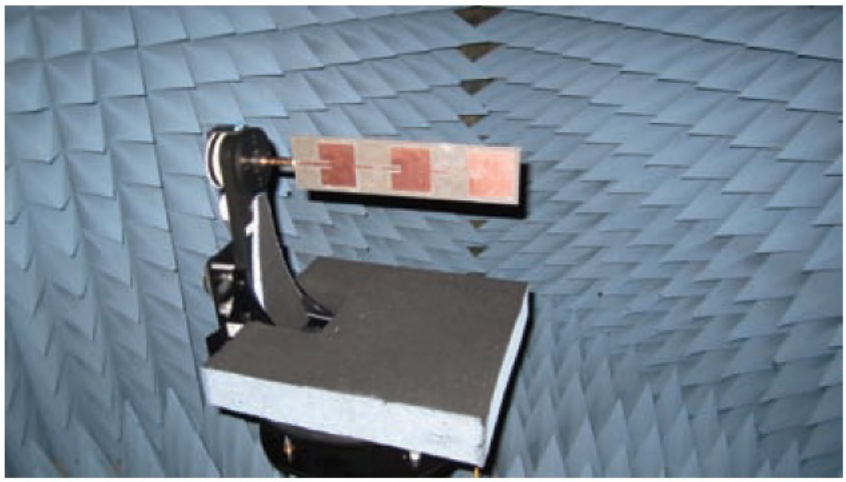

b)

Figure 17. a) Picture of the manufactured prototype and b) picture of the manufactured prototype being measured in the anechoic chamber.

a dielectric constant of 2.2 and a loss tangent of 0.0009. Method-of-moment based Agilent-ADS Momentum [54] was used for design and simulations. All the measurements for the manufactured prototype antenna array were carried out in a fully calibrated anechoic chamber. A view of antenna array and antenna array under test is shown in Figure 17.

4.3.1. S-parameters

The results in Figure 18 shows the simulated and measured S_{11} values, and a good agreement with simulations can be observed. The measured bandwidth was 24 MHz with a center frequency of 2.45 GHz compared with the simulated bandwidth of 30 MHz with a center frequency of 2.425 GHz.

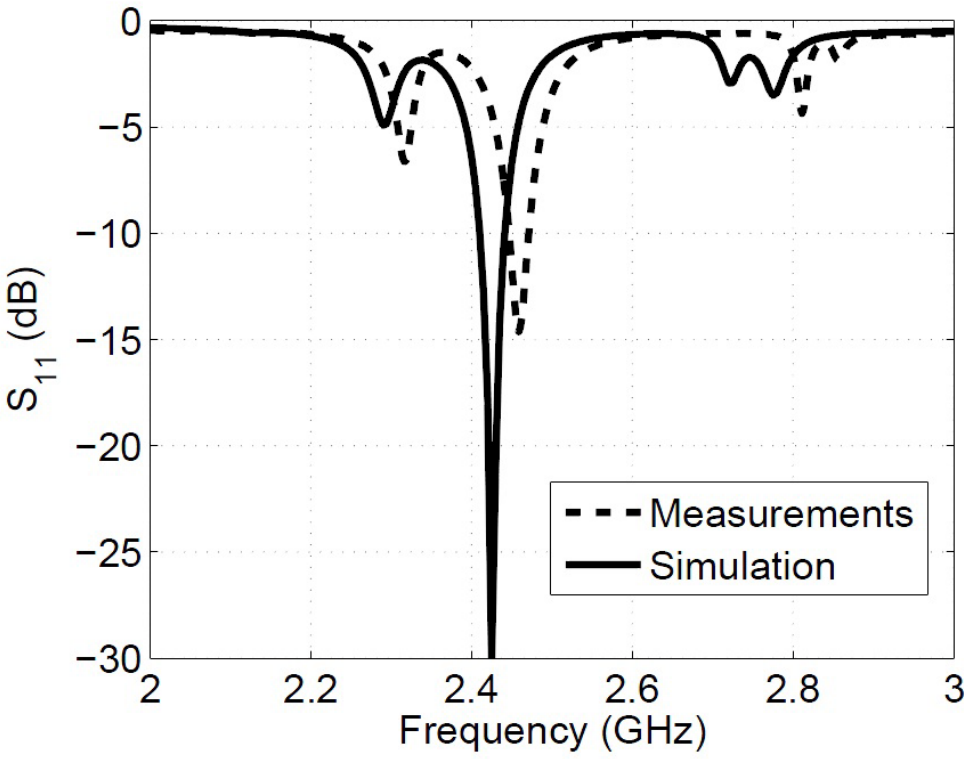

Figure 18. Simulated and measured S_{11} values.

4.3.2. Radiation pattern

Next, the radiation pattern in the x-z plane was measured and compared to

simulations. These results are shown to agree in Figure 19, and a broadside radiation pattern can be observed. The in-phase excitation of the array elements results in a broadside radiation pattern. It is also worth mentioning that the metamaterials based interconnects are more broadband as compared with the conventional transmission line interconnects. This advantage restricts the squinting of the mean lobe from broadside in radiation pattern when the array is operated above or below the operating frequency.

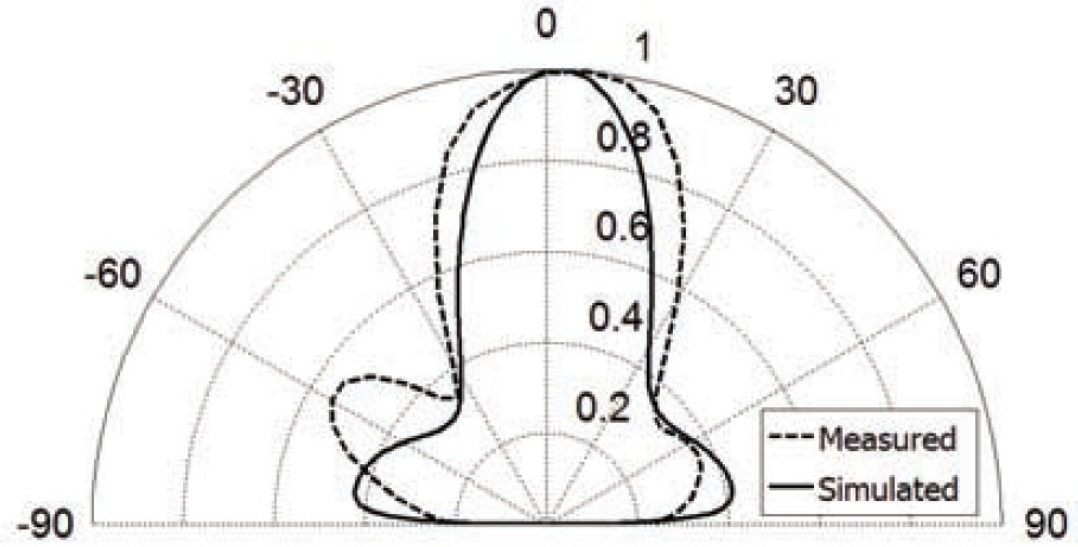

Figure 19. Measured and simulated E_θ in the x-z plane at 2.45 GHz

4.3.3. 3-D plot and surface currents

Finally, for illustration purpose, the 3-D pattern and currents on the radiating elements were computed in the simulation tool Momentum and are shown in Figure 20. The 3-D plot shows that the side lobe levels are well below the main lobe and maximum power is directed in z-direction. In the ADS simulation, a peak gain of 11 dBi was observed at the resonant frequency of the antenna array.

The surface currents were plotted at the resonant frequency and the direction of the surface currents on the patches are aligned indicating that the currents are the

same (i.e., each element is fed with the same voltage phase). The broadside series-fed antenna arrays have a tapered amplitude distribution with in phase excitation. This results in strong currents on the first antenna element and weak currents on the last antenna element.

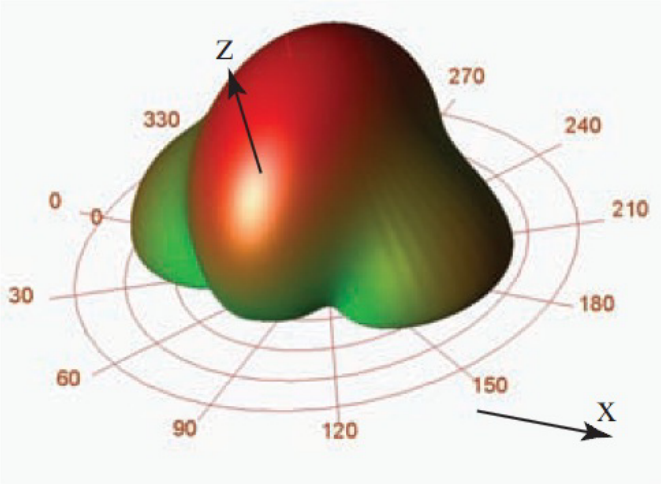

a)

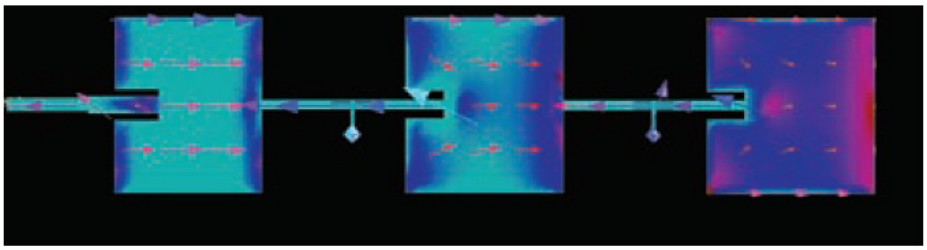

b)

Figure 20. a) Simulated 3D radiation pattern at 2.45 GHz and b) simulated surface current direction on the radiating elements at 2.45 GHz.

4.4. Summary of results

A design for a microstrip series-fed antenna array with CRLH unit-cell interconnecting lines has been presented. The array prototype was simulated in Momentum, and then manufactured and tested in an anechoic chamber. The measured results agree well with the simulated values and an impedance match can be observed at

2.45 GHz. The radiation pattern of the array has also been measured and agrees well with simulation results. Finally, the surface currents were simulated and plots show that the currents on each antenna element are in phase. Overall, the use of CRLH unit-cells in this series-fed array results in a compact design.

CHAPTER 5. A METAMATERIAL INSPIRED FREQUENCY RECONFIGURABLE SERIES-FED ARRAY

In this chapter, the benefits of frequency reconfigurable antennas and metamaterial-based transmission lines are combined to develop a frequency reconfigurable dipole antenna array. The first step in designing such arrays is the proper modeling of a reconfigurable interconnect, and by using this interconnect in series-fed antenna arrays, two-element and four-element reconfigurable dipole arrays are developed. In later sections of the chapter, the design procedure, array factor expressions and simulation and measurement results are also presented.

5.1. Introduction

Recently, there has been a significant interest in the development of antennas that are frequency, pattern and polarization reconfigurable [25]. One of the main benefits of reconfigurable antennas is that a single antenna can be used in place of multiple antennas. Furthermore, this benefit can be achieved with a smaller overall geometry because multiple antennas are not required [3]−[4]. In many of the reconfigurable antenna designs in the published literature; p-i-n diodes, RF MEMS switches and optical switches have been used to reconfigure the antennas [26]−[30]. Also, antenna designs based on metamaterials that have negative permittivity and permeability properties have gained popularity over the past decade because these characteristics can be used to design novel miniature antennas [35]−[45]. In particular, previous efforts have been made to design series-fed arrays with zero-phase interconnects to minimize the overall size and reduce beam squinting due to frequency scanning [46]−[50].

5.2. Design of reconfigurable interconnect

To implement a reconfigurable series-fed antenna array, it is important to properly design a reconfigurable interconnect in such a way that it can provide a

near to zero phase constant at two different switching frequencies. The interconnect for a series-fed antenna array was designed in ADS Momentum on a 20-mil Rogers substrate. The layout of the interconnect is shown in Figure 21.

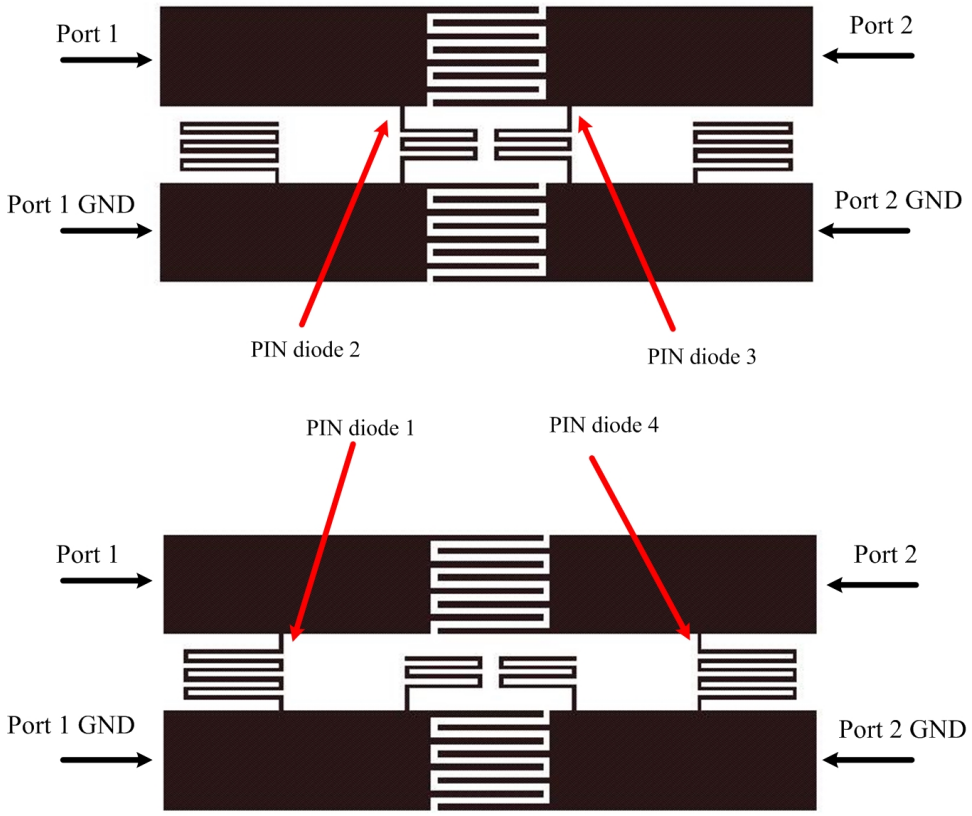

Figure 21. Layout of the proposed interconnect in ADS Momentum.

The meandered transmission lines between the upper and lower co-planar strip provide the required shunt inductance and the interdigitaed fingers in the center of the interconnect geometry provide the series capacitance. The copper trace provides the series inductance while the spacing between the upper and lower trace provides the shunt capacitance. These four parameters constitutes the required circuit elements for a CRLH design shown in Figure 7. Based upon the numerical values of these parameters, the structure can provide a negative, positive or zero phase delay at the designed frequency of interest. For this work, it is required that at the first switching

instant, the outer meandered inductors are turned on for providing the zero-phase delay at the lower frequency of operation, and at the other switching instant, the inner meandered conductors provide the required zero-phase delay at a higher frequency. In ADS Momentum simulation, copper strips were used to replace RF p-i-n diodes to switch between the two shunt inductors. Figure 22 shows the magnitude of S_{11} for two switching frequencies. An $|S_{11}|$ of more than -20 dB can be observed in both switching bands of 1.9 GHz and 2.49 GHz showing that the reflections are very low and the power is transmitted towards the output port. The magnitude response of S_{21} shown in Figure 23 depicts that the output power level is within -3 dB range for frequencies of 1.9 GHz and 2.49 GHz. Next, the phase response of S_{21} was plotted for two switching configurations and is shown in Figure 24. The zero crossing for the lower switching band is around 2 GHz and for the upper switching band the zero phase crossing is around 2.5 GHz.

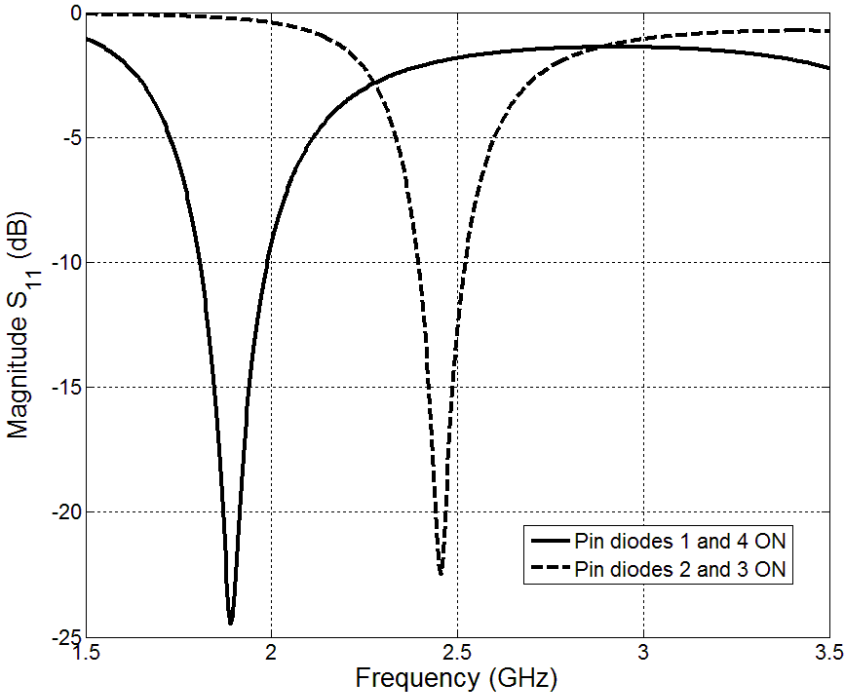

Figure 22. Magnitude of the S_{11} for two configurations.

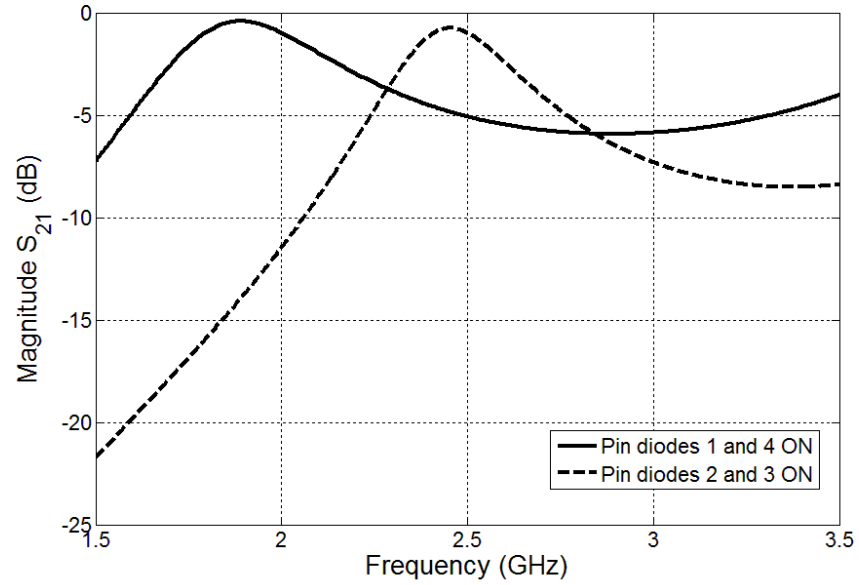

Figure 23. Magnitude of the S_{21} for two configurations.

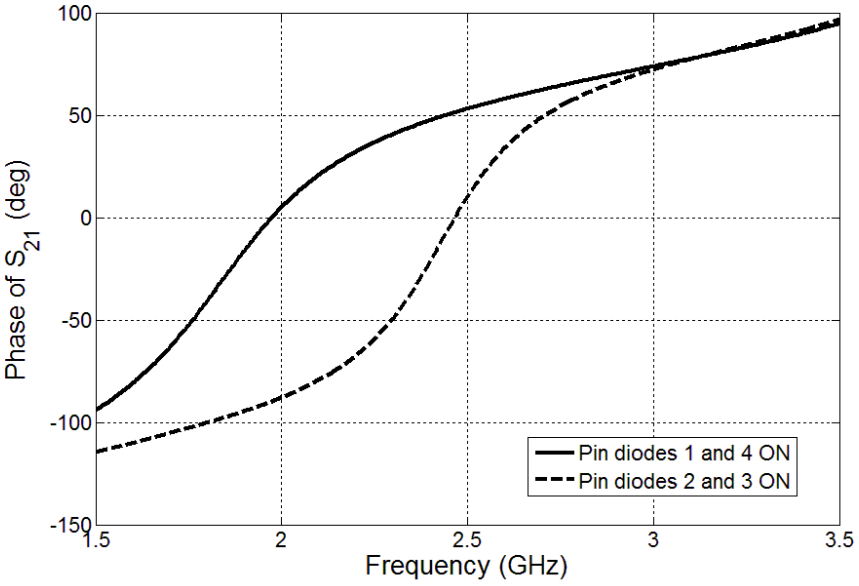

Figure 24. Phase response of S_{21} depicts zero-phase at two designed frequencies.

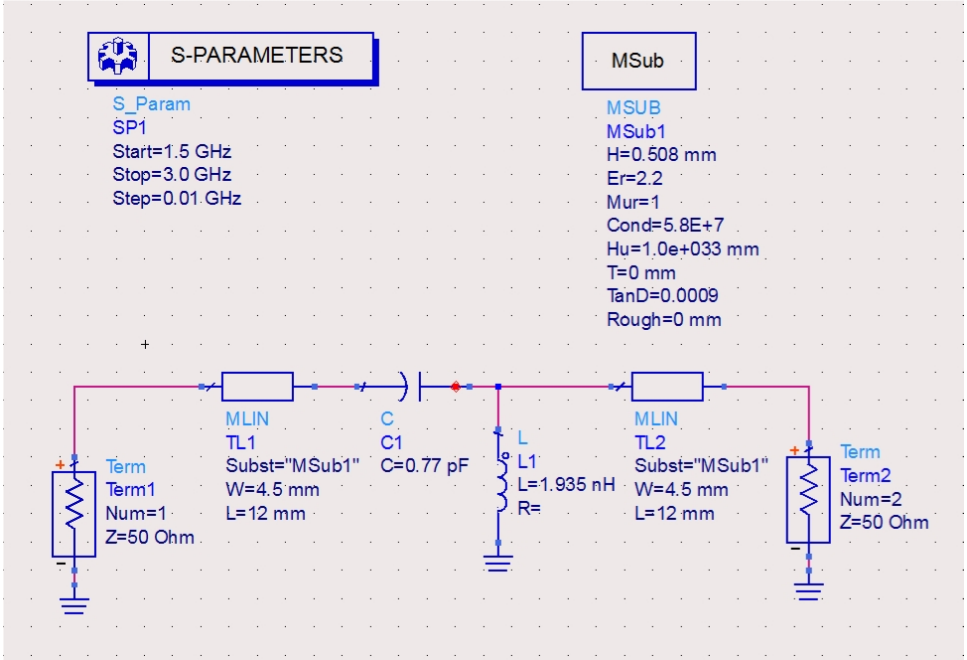

Figure 25. Circuit simulation in ADS.

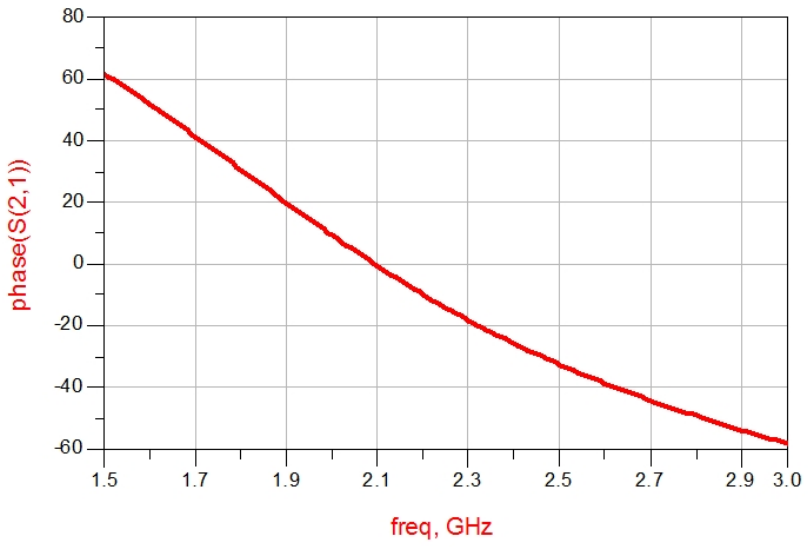

Figure 26. Phase of S_{21} at 2.1 GHz.

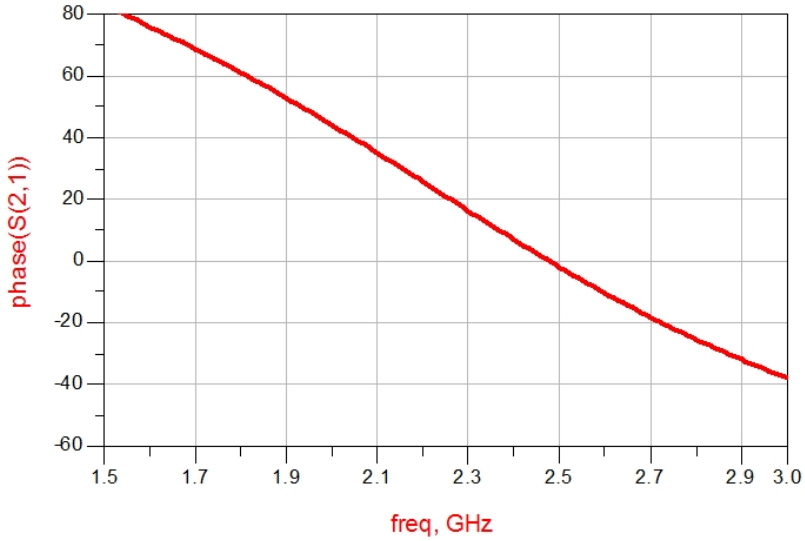

Figure 27. Phase of S_{21} at 2.5 GHz.

The interconnect shown in Figure 21 has an inductor finger spacing and finger width of 0.2 mm. In order to meet the manufacturing limitations for the final layout of the series-fed antenna array with the reconfigurable interconnect, the spacing between the inductor fingers was set to 0.25 mm and the finger length was slightly increased to place the RF p-i-n diodes. The outer meandered inductor was slightly adjusted between the upper and lower copper traces and this shifted the S_{21} phase around 2.1 GHz. The two-element and four-element reconfigurable array design explained in next sections have the lower switching frequency of 2.1 GHz.

Next, the parametric values of shunt inductance and series capacitance were extracted from the S-parameter data. These values where used in an ADS circuit simulation to plot the S_{21} phase response of the interconnect used in the reconfigurable array. A screen shot of the ADS circuit simulation is shown in Figure 25. The parametric values were slightly optimized to get the required phase at the frequencies of interest. The phase response of S_{21} for lower and upper switching frequencies is

shown in Figure 26 and Figure 27 which are in a very close agreement with the phase response shown in Figure 24.

5.3. Two-element array

In order to demonstrate the switching capability of RF p-i-n diodes, the array was first implemented using two dipole elements. The length of dipole arms were controlled using forward and reverse biasing of the p-i-n diodes. In ADS Momentum simulation, differential ports were used to feed the array. A photograph of the manufactured two-element array is shown in Figure 28.

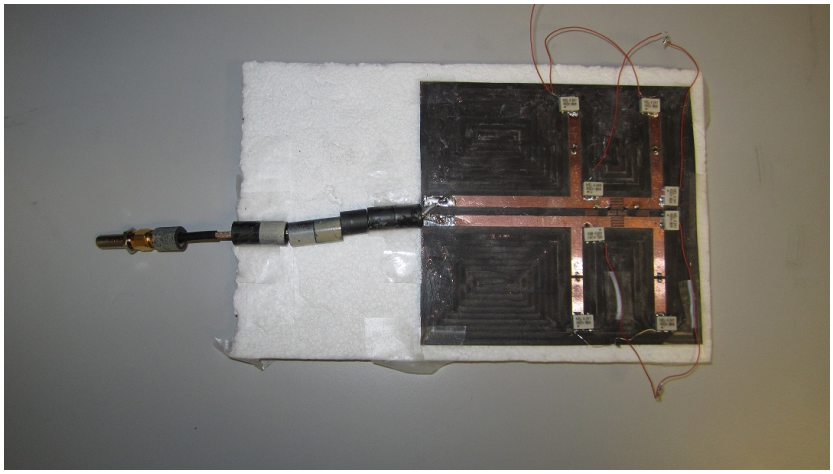

Figure 28. Photograph of the fabricated two-element reconfigurable metamaterial dipole array.

The coaxial cable was used to feed the manufactured prototype array in such a way that its inner conductor was soldered to the upper copper trace and outer conductor was soldered to the lower copper trace. The ferrite beads were used around the coaxial cable in a way reported in [47] to perform an unbalanced to balanced transformation. This is an inexpensive way of implementing a broadband balun, and it chokes off the unwanted currents flowing on the outer conductor. The effectiveness of such a feeding technique is demonstrated in [47]. For illustration purpose, a two-port transmission line was attached to a FR4 substrate in the manner shown in Figure 29 and Figure 30, and the measured results of the magnitude of S_{21} using a network

analyzer are shown in Figure 31. A -6 dB drop in magnitude can be observed when the wire is wrapped with a ferrite bead as compared to the wire without a ferrite bead.

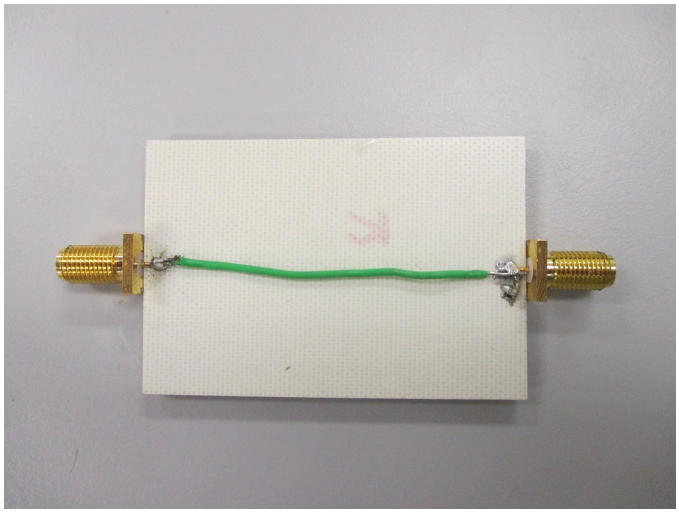

Figure 29. A two-port transmission line on a FR4 substrate with no ferrite bead.

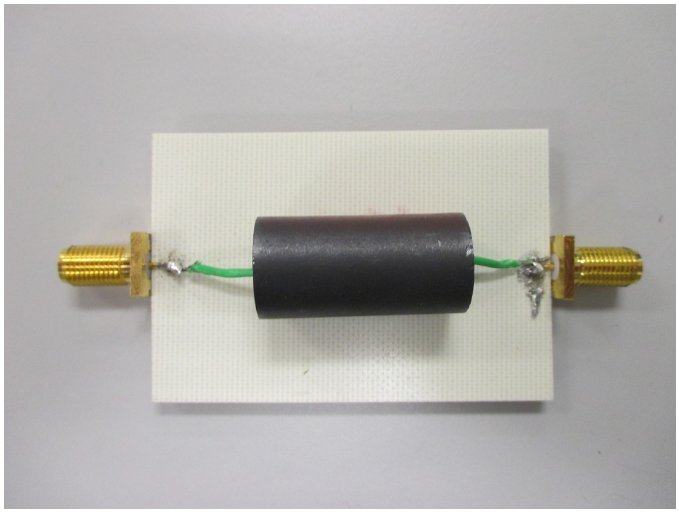

Figure 30. A two-port transmission line on a FR4 substrate with a ferrite bead.

The return loss for the manufactured two element array was measured in an anechoic chamber and the array under test is shown in Figure 32. In Figure 21, when the p-i-n diodes 1 and 4 are forward biased and p-i-n diodes 2 and 3 are reverse biased, the array resonates at around 2.1 GHz and when the p-i-n diodes 2 and 3 are forward

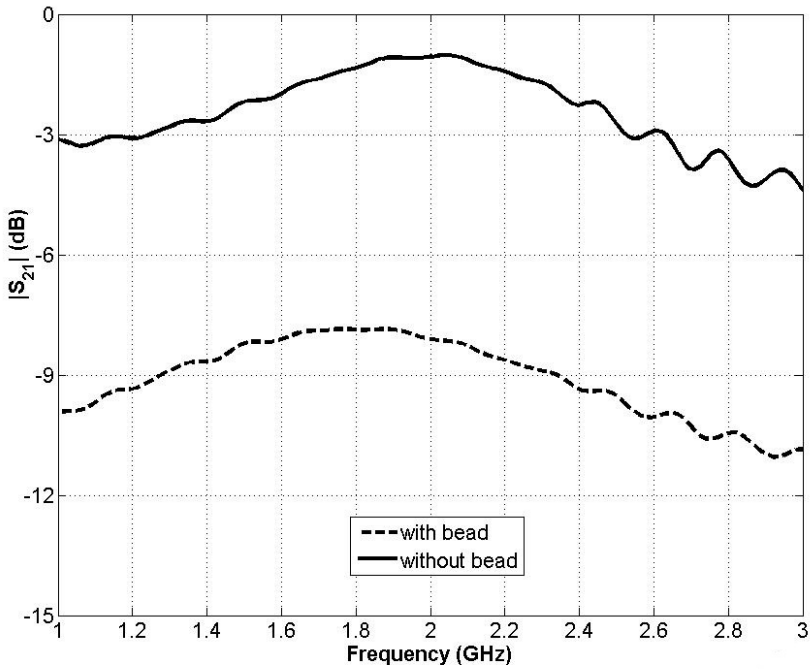

Figure 31. The magnitude of S_{21} with and without ferrite bead.

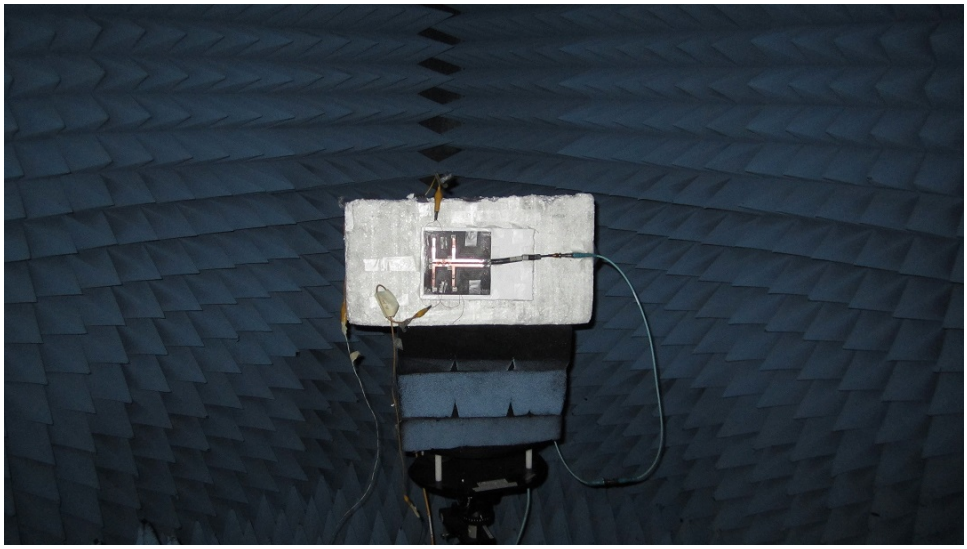

Figure 32. Two-element reconfigurable metamaterial dipole array under test in anechoic chamber.

biased and the p-i-n diodes 1 and 4 are reverse biased the array resonates at around 2.35 GHz. A very close agreement between the simulated and measured return loss can be observed in Figure 33. Next, the simulated E_ϕ component of the radiation pattern in the x-z plane is plotted in Figure 34. A broadside radiation pattern can be observed in both bands.

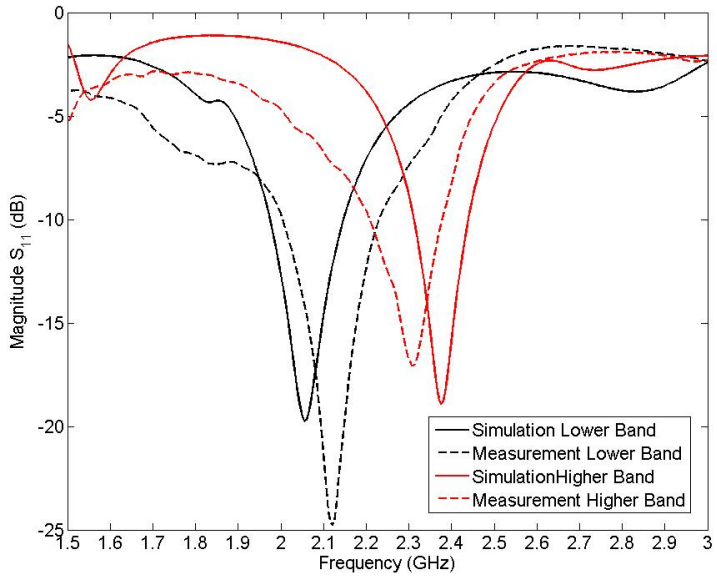

Figure 33. Simulated and measured return loss for two-element reconfigurable array.

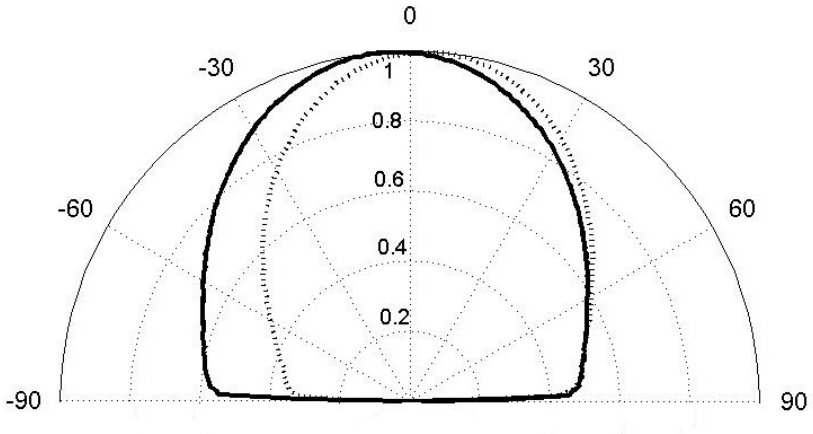

Figure 34. Simulated radiation pattern of the two-element array in the x-z plane, lower configuration (solid line) and upper configuration (dashed line).

5.4. Four-element reconfigurable metamaterial dipole array

To achieve a more directed broadside radiation pattern, the antenna array presented in the previous section was extended to a four-element design. In the following sections, the array factor theory, design procedure and simulation and measurement results of the four-element reconfigurable antenna arrays are discussed.

5.4.1. Theory

In order to get a broadside radiation pattern, for series-fed antenna array applications, all elements in the array require the same feeding phase. This requires that the interconnects between array elements should be separated by one guide wavelength λ_g at the operating frequency which will ensure a phase delay of -2π for the next antenna element. Traditionally a $\lambda_o/2$ spacing is used between antenna elements to reduce mutual coupling and avoid grating lobes in the radiation pattern.

The layout of the proposed antenna is shown in Figure 35 (a) and consists of a reconfigurable composite right-/left-handed (CRLH) transmission lines (TLs) as the interconnections between four reconfigurable dipoles. For this work, broadside radiation is assumed at the switching frequencies of 2.1 GHz and 2.5 GHz. To provide this broadside radiation at each frequency, the reconfigurable zero-phase CRLH-TL shown in Figure 35(b) was designed to provide each element in the array with the same voltage phase. The overall structure is a co-planar strip (CPS). The series capacitance is introduced with interdigitated fingers and the shunt inductance between conductors is introduced with meander-lines. To enable reconfigurability into the design, p-i-n diodes (denoted as D_1, D_2, D_3 and D_4) are used to control which meander-line is used to provide the inductance between the conductors. The manner in which this inductance is controlled is the following: when a positive voltage is applied to the top conductor (and the bottom conductor is a reference), then diodes D_2 and D_3 are biased and the meander-lines closest to the interdigital capacitor (IDC) are used

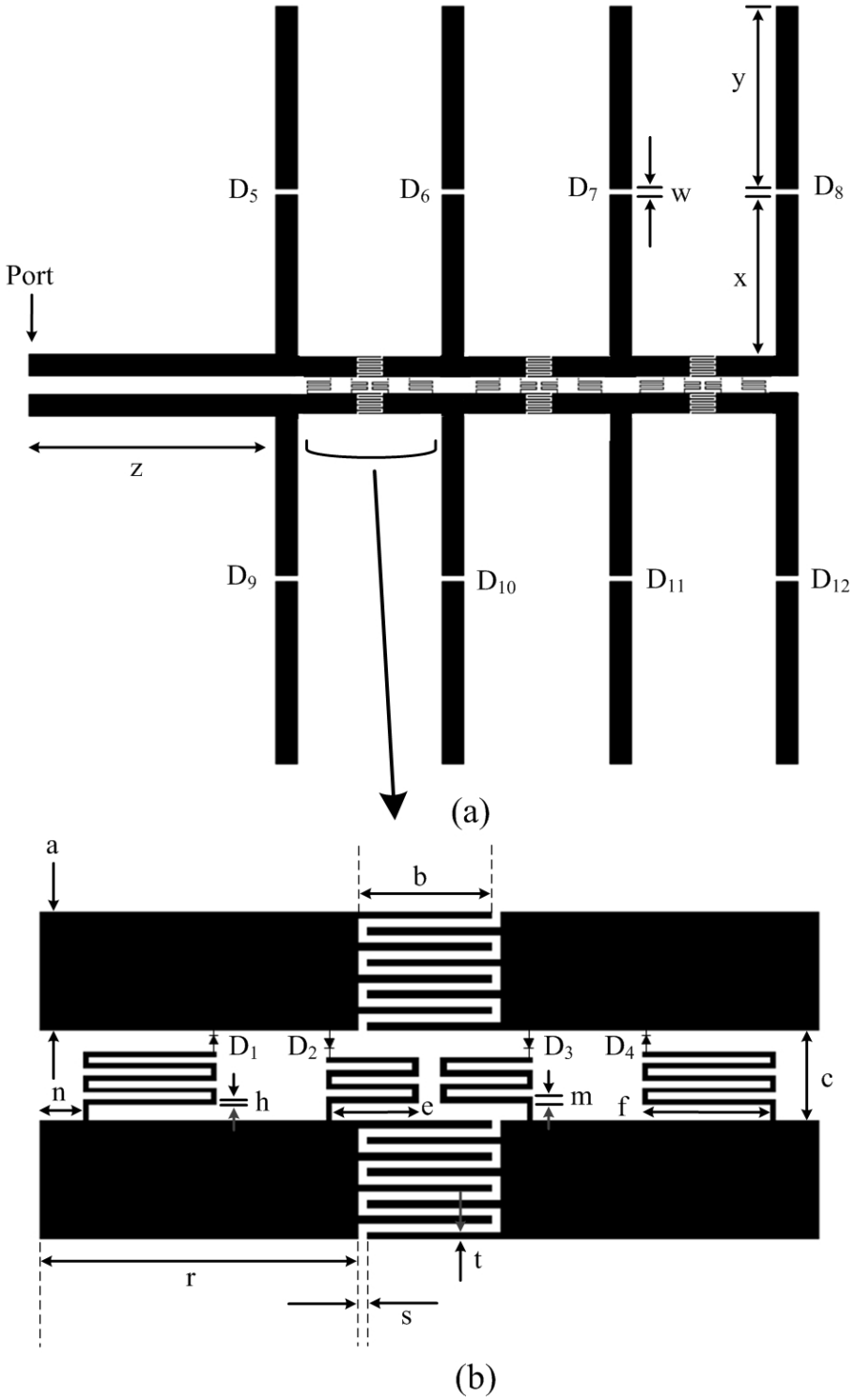

Figure 35. (a) Layout of the proposed reconfigurable series-fed array and (b) layout details of the reconfigurable zero-phase CRLH-TL interconnects (a = 4.5 mm, b = 5.0 mm, c = 3.4 mm, e = 3.25 mm, f = 4.8 mm, h = 0.2 mm, m = 0.25 mm, n = 1.65 mm, r = 12.0 mm, s = 0.3 mm, t = 0.3 mm, w = 1.0 mm, x = 32.5 mm, y = 37.0 mm and z = 50.0 mm).

to introduce inductance. This then sets the upper zero-phase frequency. Then, to switch the zero-phase frequency of the CRLH interconnect, a negative voltage is applied to the top conductor. This then results in reverse-biased diodes D_2 and D_3 and forward-biased diodes D_1 and D_4. This then disconnects the meander-lines closest to the IDC and connects the meander-lines between the conductors further away from the IDC. The result is a second lower zero-phase frequency. Finally, the frequency reconfigurable characteristics of the dipoles are achieved by introducing diodes along the length of each arm (shown in Figure 35(a) as D_5 - D_{12}). For lower-operating frequencies, the diodes are biased, and for upper-operating frequencies, the diodes are unbiased. The lower- and upper-operating frequencies correspond to the zero-phase frequencies of the interconnecting CRLH-TLs.

For this design, the two switching frequencies of $f_{o_1} = 2.1$ GHz and $f_{o_2} = 2.5$ GHz have a wavelength of $\lambda_{o_1} = 142.8$ mm and $\lambda_{o_2} = 120$ mm, respectively. Then, to reduce the overall size of the array, the interconnect lengths between the array elements were defined to be 30 mm. This then results in a $\lambda_{o_2}/4$ spacing at 2.5 GHz and a $\lambda_{o_1}/5$ spacing at 2.1 GHz.

The array factor expressions for the lower-band configuration and the upper-band configuration are expressed as,

$$AF_{\lambda_o/5} = \frac{1}{N}\sum_{q=0}^{N-1} a_n e^{jq\phi_{CRLH}} e^{-jk(2q+1-N)\lambda_{o_2}\cos\phi/10}, \tag{5.1}$$

and

$$AF_{\lambda_o/4} = \frac{1}{N}\sum_{q=0}^{N-1} a_n e^{jq\phi_{CRLH}} e^{-jk(2q+1-N)\lambda_{o_2}\cos\phi/8}. \tag{5.2}$$

In the above equations, ϕ_{CRLH} is the phase due to the right-/left handed transmission line segment and λ_{o1} and λ_{o2} represent the two operating wavelengths. The loading element values for series capacitance and shunt inductance (C_o and L_o) can be computed using expressions found in [47] and [48]. From the CRLH transmission line theory the phase response is calculated using the individual phase responses of right hand and left hand portion of the transmission lines as,

$$\phi_{total} = \phi_R + \phi_L \tag{5.3}$$

From the final design of the interconnect in ADS Momentum, the computed loading element values for the lower band configuration were $C_o = 0.56$ pF and $L_o = 1.403$ nH and for the upper band configuration the values were $C_o = 0.43$ pF and $L_o = 1.09$ nH. The above values were computed using the equations given below [47]−[48]:

$$L_o(f_{1,2}) = Z_o \times (\frac{1}{2 \times \omega_o \times \phi_L}) \tag{5.4}$$

and

$$C_o(f_{1,2}) = \frac{1}{Z_o} \times (\frac{1}{2 \times \omega_o \times \phi_L}). \tag{5.5}$$

The above calculated loading element values were used in the ADS circuit simulation, and the phase of S_{21} was plotted to demonstrate the zero crossing at our desired frequency of operation (Figure 25).

5.4.2. Prototype simulation and experimental results

Next, a prototype of the array shown in Figure 35 was designed using (5.1) and (5.2), manufactured and tested. A picture of the manufactured prototype is shown in Figure 36 and a closer image of the CRLH interconnect is shown in Figure 37. The series-fed antenna array prototype was implemented on a 20-mil (0.508 mm) thick

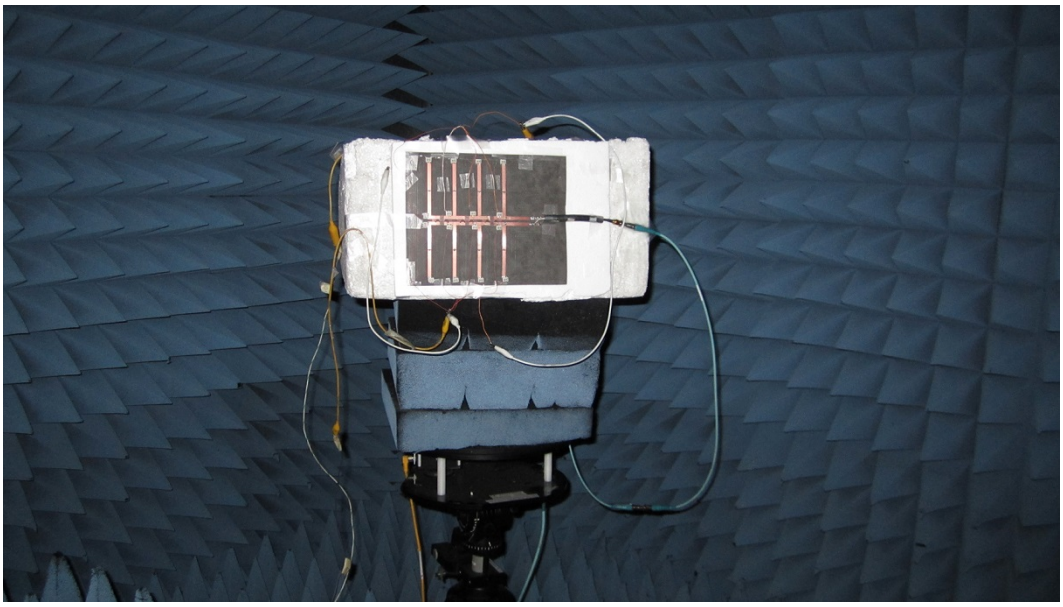

Figure 36. Photograph of the manufactured prototype array being tested in the full anechoic chamber.

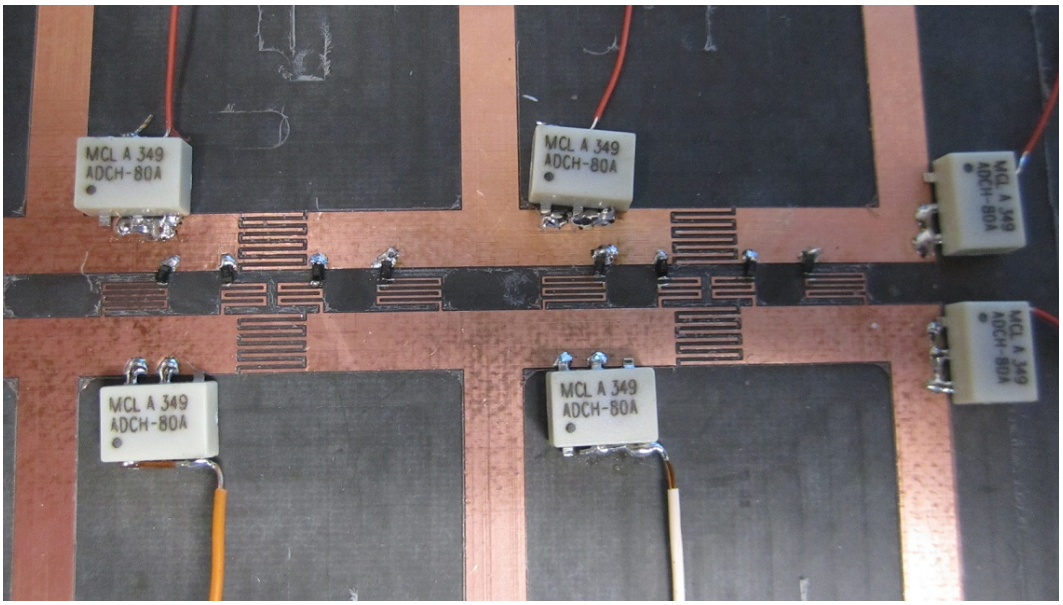

Figure 37. Photograph of the reconfigurable zero-phase CRLH-TL section.

Rogers RT/duroid 5880 [55] ungrounded (single-sided copper) substrate which has a dielectric constant of 2.2 and a loss tangent of 0.0009.

ADS Momentum [54] was used for design and simulations. The RF p-i-n diode operation in ADS was modeled using a copper strip of 1×1 mm. In ADS, the copper strip acts as a short-circuit conductor which represents the forward bias diodes, and the conductor was removed to model the reverse bias diodes. For diodes with sufficient forward and reverse bias voltages, the validity of this circuit model is shown in [49]. From the final design of the interconnect in ADS, the computed loading element values for the lower-band configuration were $C_o = 0.56$ pF and $L_o = 1.403$ nH and for the upper-band configuration the values were determined to be $C_o = 0.43$ pF and $L_o = 1.09$ nH.

Finally, the BAR50-02V RF p-i-n diodes manufactured by Infineon [56] were used on the array. To isolate the series-fed antenna array from the DC power source supplying the bias voltages, Mini-circuits ADCH-80A 10 GHz RF Chokes [57] were used.

5.4.3. Surface currents on the array

As an initial step to illustrate the radiating properties of the array, the surface currents on the radiating dipoles were computed using the post processing tool in ADS and these results are shown in Figure 38 to Figure 41. When the array is reconfigured to the lower-band, the black arrows in Figure 38 show that the current on the dipoles are in the same direction and construct to provide a desired far-field pattern. The array was then driven at 2.5 GHz in ADS and the configuration was left in the lower-band. The current results for this case are shown in Figure 39. The total currents on the dipole arms are not all in the same direction indicating a destructive far-field and a reduction in gain. This also indicates that each element is not fed with the same phase. Next, the array was reconfigured in ADS to operate in the upper-band

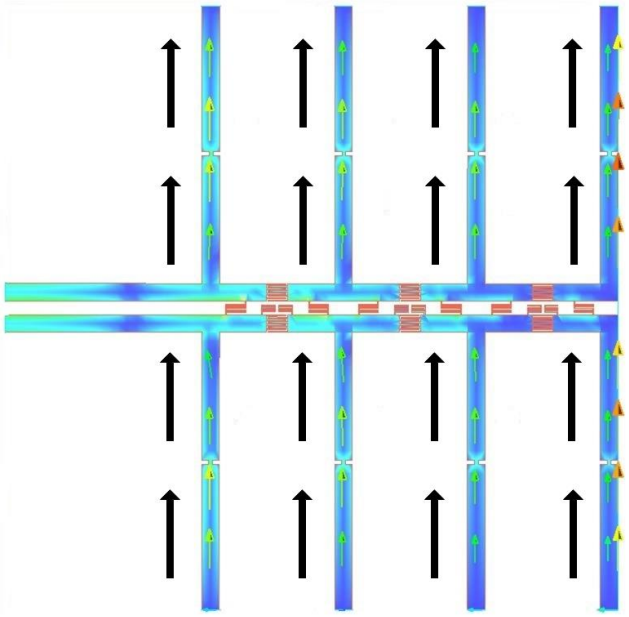

Figure 38. Surface currents at 2.12 GHz with the antenna reconfigured to the lower-band.

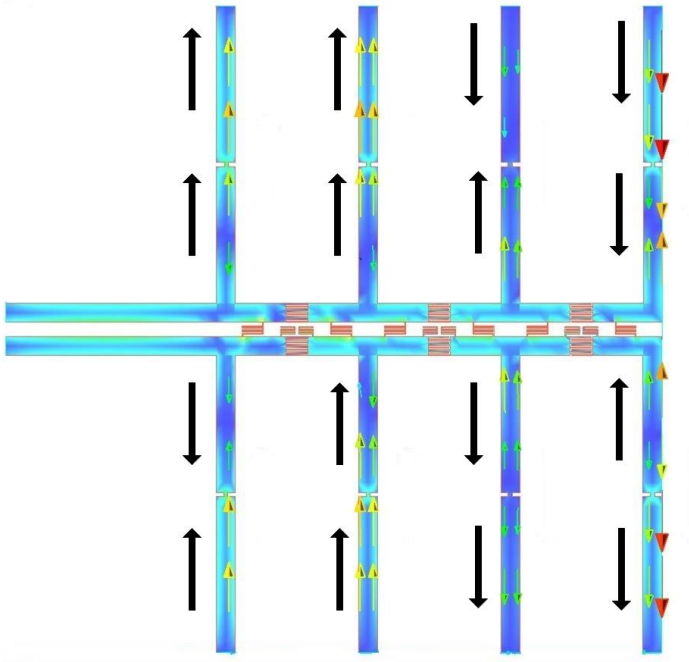

Figure 39. Surface currents at 2.5 GHz with the antenna reconfigured to the lower-band.

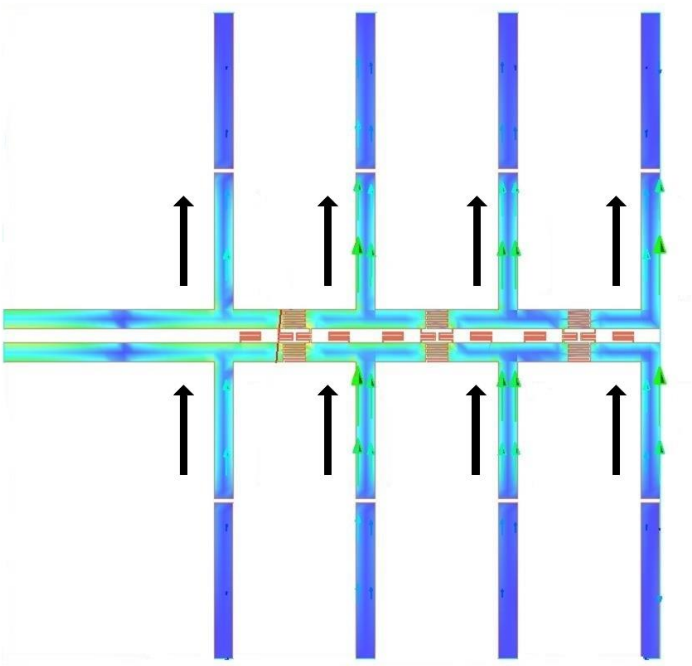

Figure 40. Surface currents at 2.5 GHz with the antenna reconfigured to the upper-band.

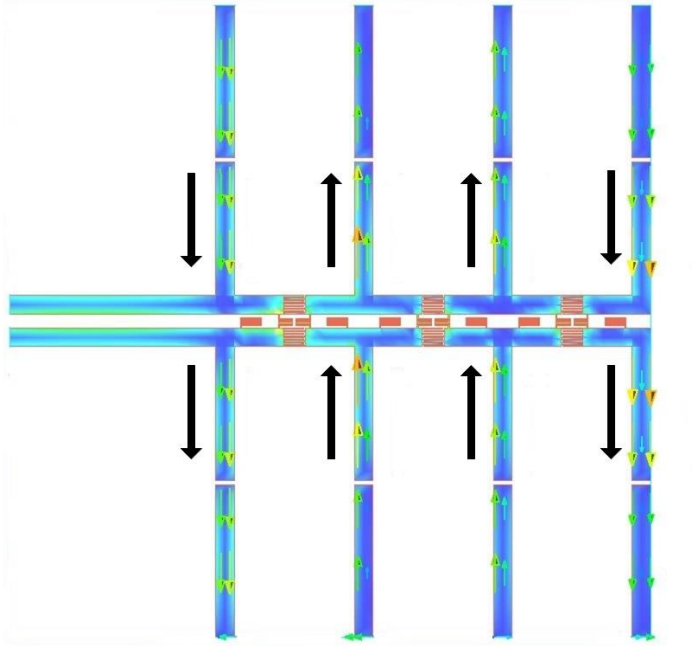

Figure 41. Surface currents at 2.12 GHz with the antenna reconfigured to the upper-band.

and driven at 2.5 GHz and 2.12 GHz. The results from these simulations are shown in Figure 40 and Figure 41, respectively. Again, the currents at the reconfigured upper-band are in the same direction and contribute to a far-field with higher gain.

5.4.4. S-parameters

Next, the prototype antenna in Figure 36 was placed in a full anechoic chamber and the S-parameters were measured. The results from these measurements are shown in Figure 42 and Figure. 43 for the antenna frequency reconfigured for the lower- and upper-bands, respectively.

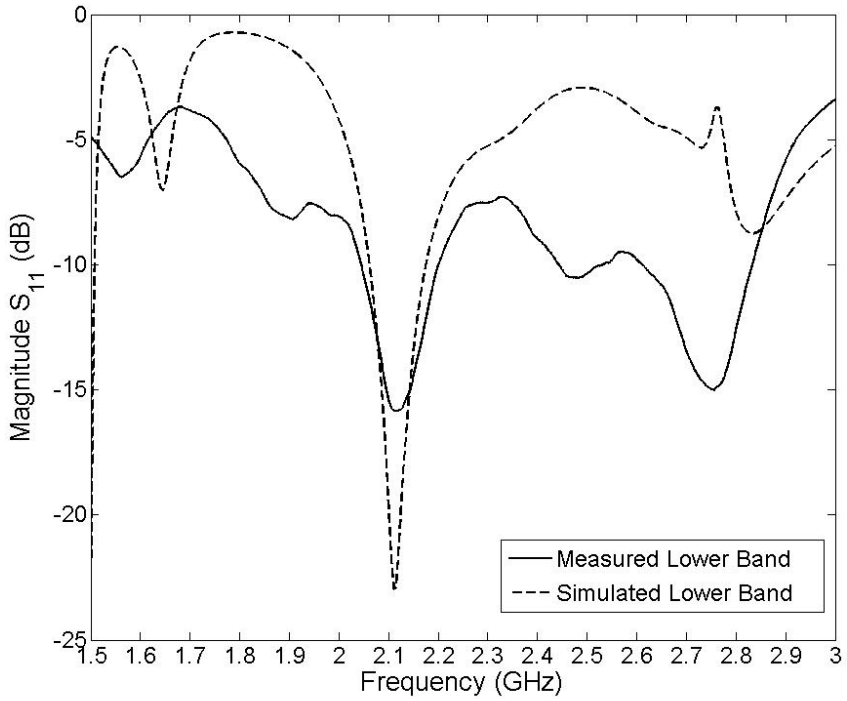

Figure 42. Simulated and measured $|S_{11}|$ for the lower-frequency reconfigurable band.

The simulated S_{11} magnitude response values for the lower- and upper-bands along with the no-bias condition are also shown in Figure 44 for comparison. Good agreement between measurements and simulations are shown. For the lower-band, the simulation results show a -10 dB bandwidth from 2.06 GHz to 2.18 GHz, and the measured data reveals a -10 dB bandwidth from 2.045 GHz to 2.2 GHz. For the

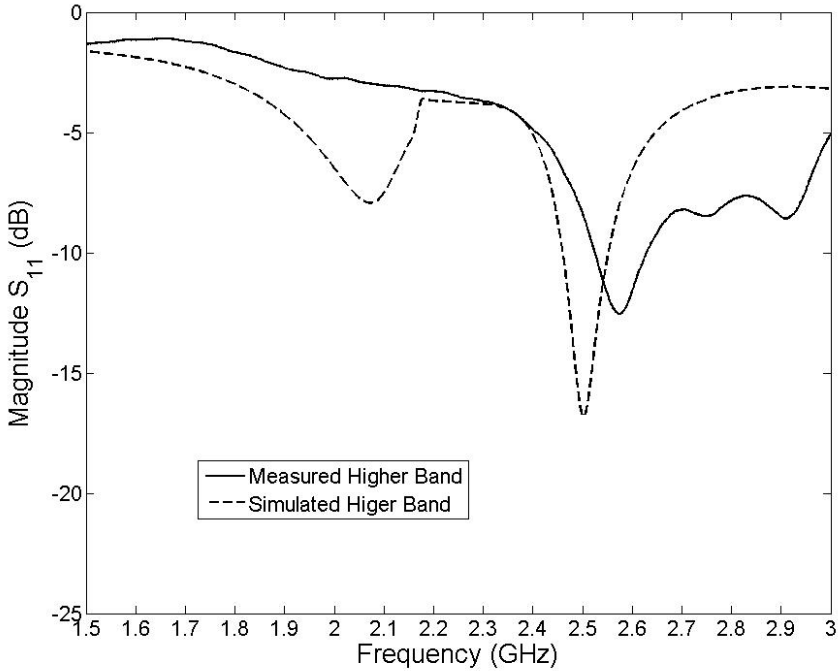

Figure 43. Simulated and measured $|S_{11}|$ for the upper-frequency reconfigurable band.

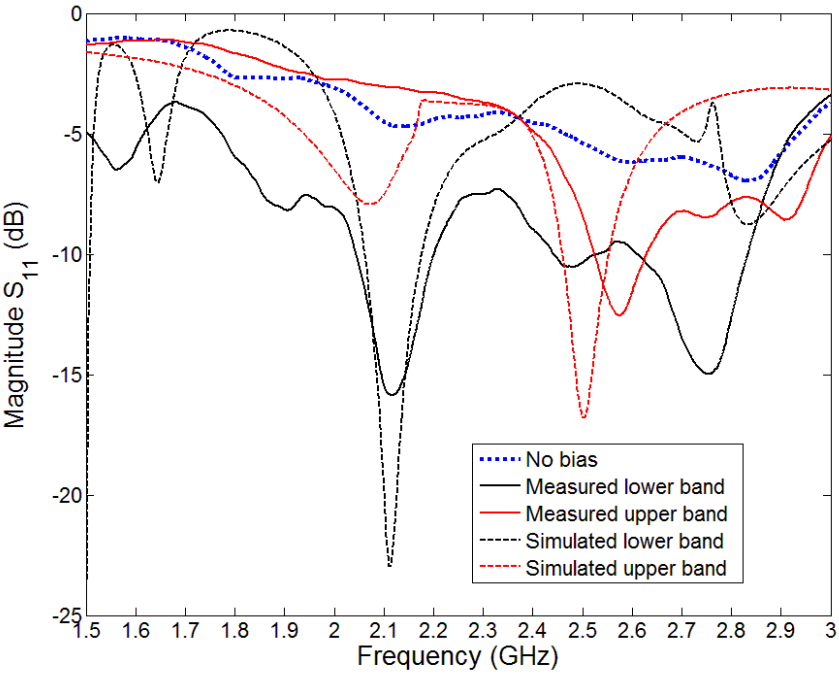

Figure 44. Simulated and measured $|S_{11}|$ for the lower-frequency reconfigurable band and upper-frequency reconfigurable band including no-bias condition.

upper-band configuration, the simulated -10 dB bandwidth is from 2.46 GHz to 2.55 GHz, and the measured data shows a -10 dB bandwidth from 2.52 GHz to 2.63 GHz.

5.4.5. Radiation pattern

Next, the radiation pattern of the array was measured in both the lower- and upper-operating bands. In particular, the E_ϕ component in the x-z plane was measured at 2.12 GHz and 2.57 GHz. The results from these measurements are shown in Figure 45 and Figure 46, respectively. For the lower-operating band, the main lobe of the simulated radiation pattern is 5 degrees off broadside, and the main lobe of the measured radiation pattern is 15 degrees off broadside. This pattern shift is thought to be due to (1) the loading parasitics introduced by the p-i-n diodes along the CPS-TL and (2) the manufacturing imperfections of the array interconnects. Again, at the upper-band, the simulation shows the main lobe is 9 degrees off broadside and the measured radiation pattern main lobe is 18 degrees off broadside. Again, diode parasitics and manufacturing imperfection are thought to be the cause of the radiation pattern shift from broadside. Further work could be done to model the parasitic effects of the p-i-n diodes.

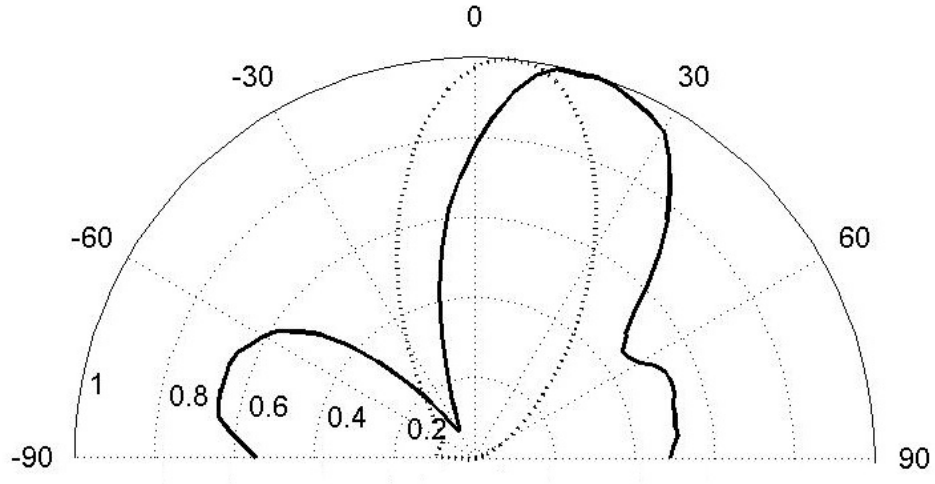

Figure 45. Simulated (dashed line) and measured (solid line) radiation pattern of E_ϕ in the x-z plane at 2.12 GHz.

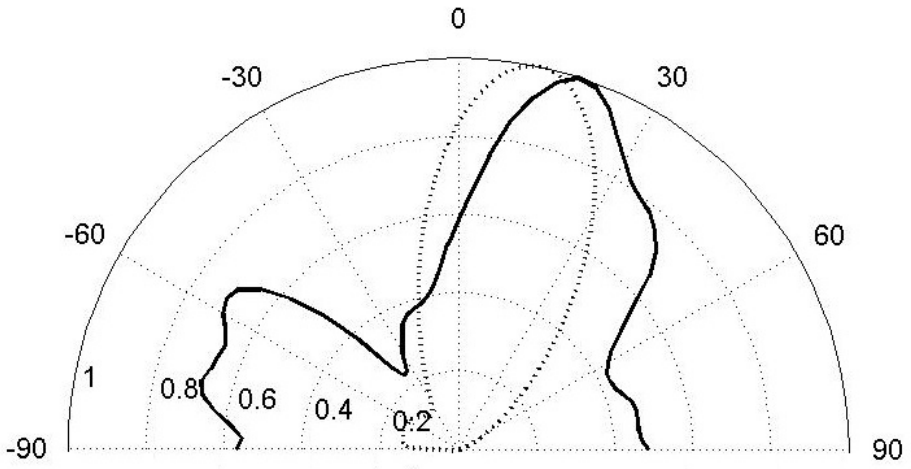

Figure 46. Simulated (dashed line) and measured (solid line) radiation pattern of E_ϕ in the x-z plane at 2.57 GHz.

5.4.6. Gain

Next, the gain of the reconfigurable antenna array was measured in a fully calibrated anechoic chamber. The gain values recorded in the anechoic chamber were then compared to the simulated gain values which showed useful results and the limitations of applying RF p-i-n diodes to an array. For the lower-band configuration of the array, the measured gain was 2.1 dBi at 2.12 GHz, -4.1 dBi at 2.57 GHz and -6.8 dBi at 2.7 GHz. For the upper-band configuration, a gain of 2.1 dBi was measured at the resonant frequency of 2.57 GHz. Also for the same configuration the measured gain values at 2.12 GHz and 2.7 GHz were -11.7 dBi and -4.2 dBi, respectively. The ADS simulated gain was around 6.8 dBi at both resonant frequencies. The measured gain was 4.7 dBi below the simulated gain. This is due to the active diodes present on the antenna geometry. For illustration purposes the diodes in the manufactured prototype were replaced by copper tape, and a gain of 6.7 dBi was measured in the fully calibrated anechoic chamber in the direction of peak radiation. The gain values with copper tape closely match the gain values of ADS momentum. Thus, one drawback of using RF p-i-n diodes on an antenna array is the drop in gain; however,

the array showed reasonable gain at both switching frequencies. The measured gain values are also expressed in Table 2 and Table 3 for both switching configurations.

Table 2. Gain at lower-frequency reconfigurable band.

Frequency (GHz)	Measured gain (dBi)
2.12	2.1
2.57	-4.1
2.7	-6.8

Table 3. Gain at upper-frequency reconfigurable band.

Frequency (GHz)	Measured gain (dBi)
2.12	-11.7
2.57	2.1
2.7	-4.2

5.4.7. Discussion on scan angle and design trade-offs

For comparison between the conventional right-handed transmission lines and reconfigurable metamaterial transmission lines, the scan angles from broadside of the two switching configurations are plotted in Figure 47 using the expressions given in [47]. It can be noted that for the array to radiate at broadside the conventional right-handed transmission line has less bandwidth from -90 to +90, and it is more frequency dependent as compared to the metamaterial transmission lines. Both the angles pass through the switching frequency of 2.1 GHz and 2.5 GHz. The metamaterial interconnect is more broadband as compared to the conventional interconnect.

The reconfiguration mechanism on an antenna array depends on the overall array geometry. The introduction of any sort of mechanism such as, RF-MEMS, p-i-n diodes or optical switches will add weight, cost, losses and complexity in design. From a designer's point of view, some trade-offs in designing reconfigurable antenna arrays are fabrication complexity, implementation of bias network in tiny space available between inductor traces and the durability of the array under harsh electromagnetic environment conditions. Also, it is worth mentioning that a big shift in the operating

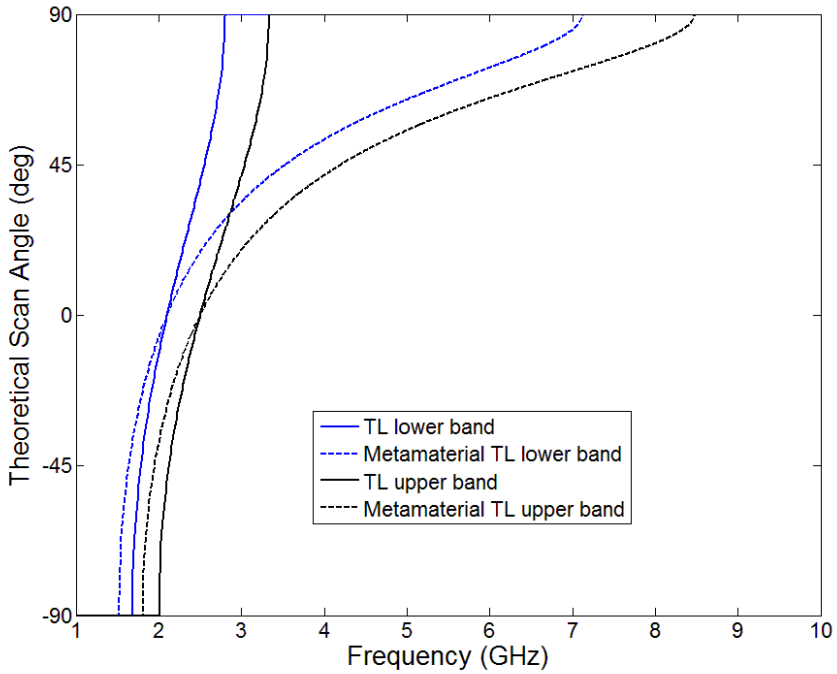

Figure 47. Scan angle for conventional and metamaterial transmission lines for both switching frequencies.

frequency can cause the matching network to give a poor input impedance match. So the impedance matching network is also a trade-off when the array is operated away from the frequency it was designed. In this research, several efforts were made in the ADS simulation environment to design the input matching network in a way that it provides reasonable agreement in impedance matching at both the switching frequencies. Also as a future work, the input matching network can be made reconfigurable, if the two switching frequencies are widely separated. However, it can be concluded that the operating functionality of a reconfigurable antenna array has an advantage over a fixed antenna array.

5.5. Summary

In this chapter, a compact frequency reconfigurable antenna array inspired by the properties of metamaterials was developed. Two meandered inductors were placed between the feed lines which were reconfigured using RF p-i-n diodes to achieve zero-

phase crossings at 2.12 GHz and 2.57 GHz. Each array element was fed with the same voltage phase at the design frequency, resulting in a near broadside radiation pattern. The fabricated antenna array has a measured bandwidth of 155 MHz at the lower-band and 110 MHz at the upper-band configuration. Owing to its unique properties, the proposed antenna array is useful in applications where broadside radiation patterns are required at both resonant frequencies, and frequency scanning is undesirable.

CHAPTER 6. CONCLUSION

In this work, the reconfigurable series-fed arrays inspired by the properties of metamaterials were presented. Chapter 1 discussed the historical development in antenna arrays along with the motivation for further research in the area. The background of linear arrays and metamaterials was presented in Chapter 2. New expressions for four element reconfigurable antenna arrays are derived in Chapter 3.

In Chapter 4, a design of a series-fed microstrip array with composite right-/left-handed transmission lines (CRLH-TLs) was proposed. To ensure that each element in the array is driven with the same voltage phase, dual-band CRLH-TLs are adopted instead of meander-line microstrip lines to provide a compact interconnect with a zero phase-constant at the frequency of operation. The simulation results of the proposed array are verified by measurements done in an anechoic chamber. A bandwidth of 24 MHz was experimentally determined with a center frequency of 2.45 GHz.

In Chapter 5, the design of a metamaterial inspired reconfigurable antenna array is presented. Devices with multi-band wireless system capabilities have significantly benefited from the introduction of frequency reconfigurable antennas. However, much of the development on frequency reconfigurable antennas has been on single antenna elements. The proposed array has the benefits of multi-band capabilities and does not scan with frequency, which is a natural occurrence in series fed-arrays due to the topology of the design. The proposed antenna consists of four reconfigurable dipoles interconnected with reconfigurable zero-phase composite right-/left-handed (CRLH) transmission lines (TLs). It is shown that instead of meander-line interconnects between the dipole elements, much more compact frequency reconfigurable CRLH-TLs can be used. RF p-i-n diodes are then used to switch between the two frequency bands of 2.1 GHz and 2.5 GHz. The developed prototype presented showed a near broadside radiation pattern at both switching frequencies, with a 155 MHz bandwidth

at the lower-switching frequency and a 110 MHz bandwidth at the upper-switching frequency. Also a maximum gain of 2.1 dBi was measured in both bands.

REFERENCES

[1] G.A. Deschamps, "Microstrip Microwave Antennas," *3rd USAF Symposium on Antennas*, 1953.

[2] David M. Pozar and Daniel H. Schaubert, "Microstrip Antennas: The analysis and Design of Microstrip Antennas and Arrays," IEEE Press, Piscataway, NJ, 1995.

[3] Warren L. Stutzman and Gary A. Thiele, *Antenna Theory and Design,* 2nd ed., John Wiley and Sons, Inc., New York, 1998.

[4] Constantine A. Balanis, *Antenna Theory: Analysis and Design,* Harper and Row, Publishers, New York, 1982.

[5] Derneryd, A., "Linearly polarized microstrip antennas," *IEEE Transactions on Antennas and Propagation,* Vol. 24, Issue 6, Nov. 1976, pp. 846-851.

[6] R.E. Munson, "Conformal microstrip antennas and microstrip phased arrays," *IEEE Transactions on Antennas and Propagation,* Vol. 22, Issue 1, January 1974, pp. 74-78.

[7] R. E. Munson, "Microstrip phased array antennas," *22nd Annual USAF Antenna Symposium,* Oct. 1972.

[8] E. Fubini. J. McDonough, and R. Malech, "Stripline radiators," *IRE Conference,* Rec., Pt. 1, p. 51, 1955.

[9] J. McDonough, R. Malech. and J. Kowalsky, "Recent developments in the study of printed antennas," *IRE Conference,* Rec., Pt. 1 , p. 173. 1957.

[10] J. R. James and C. J. Wilson, "Radiation characteristics of stripline antennas," *in Proc. 4th European Microwave Conference,* Sept. 1974, pp. 484-488.

[11] E. V. Byron, "A new flush-mounted antenna element for phased array application," *in Proc. Phased Array Antenna Symposium,* 1970. pp. 187-192, reprinted in Phased Array Antennas. A. A. Oliner and G. H. Knittel, Eds. Dedham, MA: Artech House. 1972.

[12] R. Collings, U.S. Patent 3 680 136, July 1972.

[13] C. L. Dolph, "A current distribution for broadside arrays which optimizes the relationship between beamwidth and side-lobe level," *in Proc. IRE,* vol. 34, pp. 335348 Jun. 1946.

[14] H. J. Riblet, "Discussion on A current distribution for broadside arrays which optimizes the relationship between beamwidth and side-lobe level," *in Proc. IRE,* Jun. 1947, vol. 35, pp. 489492.

[15] R. L. Pritchard, "Optimum directivity patterns for linear point arrays," *J. Acoust. Soc. Amer.,* vol. 25, pp. 879891, Sep. 1953.

[16] R. A. Sainati, *CAD of Microstrip Antennas for Wireless Applications,* Boston, MA: Artech House, 1996.

[17] Skolnik, M. I., *Introduction to RADAR System,* 3rd Edition, McGraw Hill Higher Education, 2000.

[18] Garg, R., P. Bhartia, I. Bahl, and A. Ittipiboon, *Microstrip Antenna Design Handbook,* Artech House, INC., 2001.

[19] Rodney B.Waterhouse, *Microstrip Patch Antennas A designers guide,* Kluwer Academic Publishers, 2003.

[20] T. Yuan, N. Yuan and L. Li, "A Novel Series-Fed Taper Antenna Array Design," *IEEE Antennas and Propagation Letters,* Vol. 7, pp. 362 - 365, 2008.

[21] M. Hashemi, N. Yuan and T. Itoh, "Dual-Band Composite Right/Left - Handed Metamaterial Concept," *IEEE Microwave and Wireless Components Letters,* Vol. 22, pp. 248 - 250, No. 5, May 2008.

[22] D. Schaubert, B, "Frequency-agile polarization diversity microstrip antennas and frequency scanned arrays," U.S. Patent 4 367 474, Jan. 1983.

[23] J. K. Smith, "Reconfigurable aperture antenna (RECAP)," DARPA, 1999. [Online Available]: www.darpa.mil

[24] J. Costantine, "Design, optimization and analysis of reconfigurable antennas," Ph.D. dissertation, Electr. Comput. Eng. Dept., Univ. New Mexico (UNM), Albuquerque, NM, Dec. 2009.

[25] Christos G. Christodoulou, Youssef Tawk, Steven A. Lane, and Scott R. Erwin, "Reconfigurable Antennas for Wireless and Space Applications," *Proceedings of the IEEE,* Vol. 100, No. 7, July 2012.

[26] C. W. Jung, M. Lee, G. P. Li, and F. De Flaviis, "Reconfigurable scan-beam single-arm spiral antenna integrated with RF-MEMS switches," *IEEE Trans. Antennas Propag.,* vol. 54, no. 2, pp. 455-463, Feb. 2006.

[27] S. Shelley, J. Costantine, C. G. Christodoulou, D. E. Anagnostou, and J. C. Lyke, "FPGA-controlled switch-reconfigured antenna," *IEEE Antennas Wireless Propag. Lett.,* vol. 9, pp. 355-358, 2010.

[28] C. R. White and G. M. Rebeiz, "Single and dual-polarized tunable slot-ring antennas," *IEEE Trans. Antennas Propag.,* vol. 57, no. 1, pp. 19-26, Jan. 2009.

[29] C. J. Panagamuwa, A. Chauraya, and J. C. Vardaxoglou, "Frequency and beam reconfigurable antenna using photoconductive switches," *IEEE Trans. Antennas Propag.,* vol. 54, no. 2, pp. 449-454, Feb. 2006..

[30] Y. Tawk, A. R. Albrecht, S. Hemmady, G. Balakrishnan, and C. G. Christodoulou, "Optically pumped frequency reconfigurable antenna design," *IEEE Antennas Wireless Propag. Lett.,* vol. 9, pp. 280-283, 2010.

[31] Y. Tawk, J. Costantine, S. E. Barbin, and C. G. Christodoulou, "Integrating laser diodes in a reconfigurable antenna system," *in Proc. SBMO/IEEE MTT-S Int. Microw. Optoelectron. Conf.,* Oct. 2011.

[32] S. Jalali Mazlouman, M. Soleimani, A. Mahanfar, C. Menon, and R. G. Vaughan, "Pattern reconfigurable square ring patch antenna actuated by hemispherical dielectric elastomer," *Electron. Lett.,* vol. 47, no. 3, pp. 164-165, Feb. 2011.

[33] D. M. Pozar, *Microwave Engineering,* 3rd. ed. John Wiley and Sons, Inc., 2005.

[34] A. Lai, C. Caloz, and T. Itoh, "Composite right/left-handed transmission line metamaterials," *IEEE Microwave Magazine,* vol. 5, issue 3, IEEE Microwave Magazine pp. 34 - 50, September 2004.

[35] C. Caloz and T. Itoh, *Electromagnetic Metamaterials,* Piscataway-Hoboken, NJ: Wiley-IEEE Press, 2005.

[36] G. V. Eleftheriades and K. G. Balmain, *Negative - Refraction Metamaterials,* Wiley-IEEE Press, 2005.

[37] V. Veselago, "The electrodynamics of substances with simultaneously negative values of ϵ and μ," *Soviet Physics Uspekhi,* vol. 10, no. 4, pp. 509-514, 1968.

[38] A. Sanada, M. Kimura, I. Awai, H. Kubo, C. Caloz, and T. Itoh, "A planar zeroth order resonator antenna using left-handed transmission line," *European Microwave Conf.,* Amsterdam, Netherlands, 2004.

[39] L. Liu, C. Caloz, and T. Itoh, "Dominant mode (DM) leaky-wave antenna with backfire-to-endfire scanning capability," *Electron. Lett.,* vol. 38, no. 23, pp. 1414-1416, 2000.

[40] Herd et al., "Frequency reconfigurable microstrip antenna array geometry which utilizes Micro-Electro-Mechanical System (MEMS) switches," U.S. Patent 6,198438 B1, Mar. 2001.

[41] James, Chin-Chang, Yongxi and Itoh, "A reconfigurable leaky-wave/patch microstrip aperture for phased-array applications," *IEEE Transactions on Microwave and Techniques,* Vol. 50, No. 8, August 2002.

[42] X. Zhao, L. Zhao, K. Huang, and C. Liu, "A Circularly Polarized Array Composed of Linear Polarized Microstrip Patches Fed by Metamaterial Transmission Line," *Journal of Electromagnetic Waves and Applications,* Vol. 25, 1545-1553, 2011.

[43] M. A. Antoniades and G. V. Eleftheriades, "A broadband series power divider using zero-degree metamaterial phase-shifting lines," *IEEE Microwave and Wireless Components Letters,* vol.15, no.11, pp. 808810, Nov. 2005.

[44] M. A. Antoniades and G. V. Eleftheriades, "Compact Linear Lead/Lag Metamaterial phase Shifters For Broadband Applications," *IEEE Antennas and Wireless Propagation Letters,* vol.2, pp. 103106, 2003.

[45] G. V. Eleftheriades and M. A. Antoniades, "Antenna applications of negative-refractive-index transmission-line (NRI-TL) structures," *IET Microwaves, An-*

tennas and Propagation, Special Issue on Metamaterials, vol. 1, no. 1, pp. 1222, Feb. 2007.

[46] M. A. Antoniades and G. V. Eleftheriades, "A metamaterial series-fed linear dipole array with reduced beam squinting," *Proc. IEEE International Symposium on Antennas and Propagation,* Albuquerque, NM, Jul. 2006, pp. 41254128.

[47] M. A. Antoniades, *Microwave Devices and Antennas based on Negative-Refractive-Index transmission lines Metamaterials,* PhD thesis, Department of Electrical and Computer Engineering, University of Toronto, 2009.

[48] T. Jang, S.-H. Hwang, Y.-S. Bang, J.-M. Kim, Y.-K. Kim, C.-W. Beak and S. Lim, "Switchable Composite Right/Left-Handed (S-CRLH) Transmission Line Using MEMS Switches," *IEEE Microwave and Wireless Components Letters,* vol.19, no.12, pp. 804806, Dec. 2009.

[49] B. D. Braaten, S. Roy, I. Ullah, S. Nariyal, B. Ijaz, M. M. Masud, S. A. Naqvi and A. Iftikhar, "A Cascaded Recongurable RH/CRLH Zero-Phase Microstrip Transmisison Line Unit Cell," *Proceedings of the IEEE International Conference on Wireless Information Technology and Systems (ICWITS),* Maui, Hawaii, Nov. 11th - 16th, 2012.

[50] Bilal Ijaz, S. Roy, M. M. Masud, A. Aftikhar, S. Nariyal, I. Ullah, K. Asirvatham, B. Booth and B. D. Braaten, "A Series-fed Microstrip Patch Array with Interconnecting CRLH Transmission Lines for WLAN Applications," *Proceedings of the 7th European Conference on Antennas and Propagation (EuCAP 2013),* pp. 2088-2091 Apr. 12 - 18, 2013, Gothenburg, Sweden.

[51] Jennifer T. Bernhard, *Reconfigurable Antennas,* Morgan and Claypool Publishers, 2007.

[52] R. Waterhouse, *Microstrip Patch Antennas: A Designers Guide,* 1st ed., Springer, 2003.

[53] M. M. Alam, M. M. R. Sonchoy and M. O. Goni, "Design and performance analysis of microstrip array antenna," *Progress in Electromagnetics Research Symposium Proceedings,* Moscow, Russia, Aug. 18 - 21, 2009.

[54] Advanced Design System (ADS) by Agilent Technologies, [Online Available]: www.agilent.com.

[55] Rogers Corporation, [Online Available]: www.rogerscorp.com.

[56] Infineon Technologies, [Online Available]: http://www.infineon.com/

[57] Mini-Circuits, [Online Available]: www.minicircuits.com